CONTENTS

FIGURES

TABLES

1 Introduction to Strong Motion

The North Coast of California is a highly seismically active area because of its proximity to the intersection of three tectonic plates: the Pacific plate to the south, the Gorda plate to the north, and the continental North America plate to the east (Oppenheimer et al., 1993; Velasco et al., 1994; Schwartz and Hubert, 1997; Furlong and Schwartz, 2004) (Figure 1).

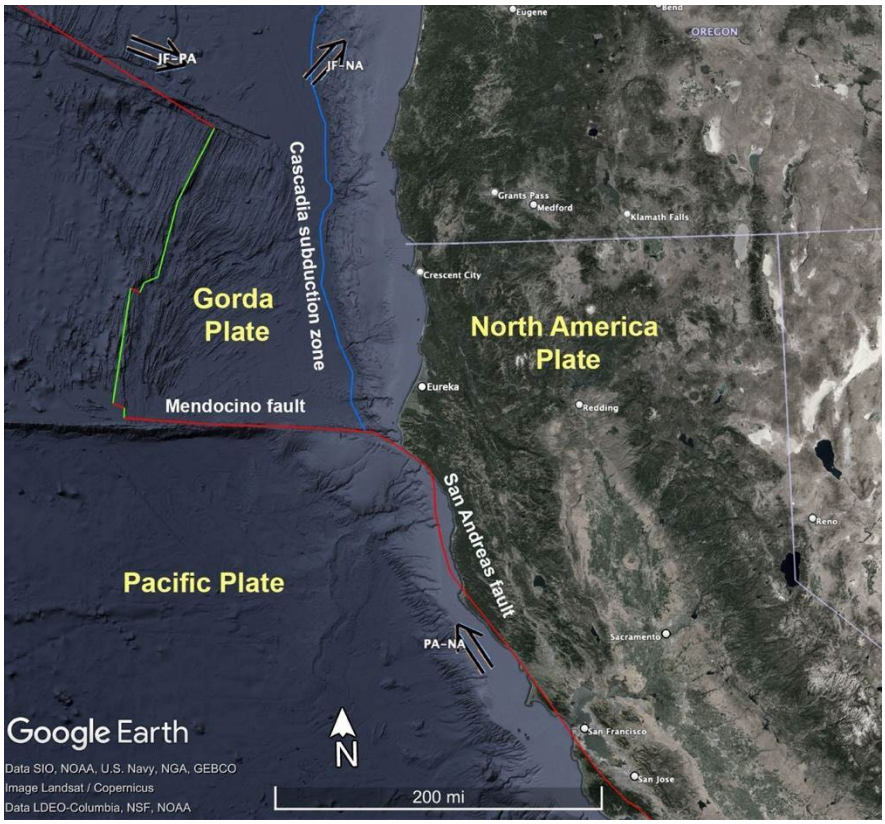

Figure 1. Map of the intersection of the Gorda, Pacific, and North America plates at the Mendocino triple junction. Plate names are indicated in yellow lettering, major plate boundaries are indicated in white lettering adjacent to boundaries (blue is contractional, red is transform, green boundary is the Gorda ridge and is extensional). Double arrows indicate plate motions, example PA-NA is the motion of the Pacific Plate with respect to North America). Boundaries and plate vectors are from USGS https://www.usgs.gov/programs/earthquake-hazards/google-earthtmkml-files

The zone where the plates meet, the Mendocino triple junction (MTJ) (Atwater, 1989; Velasco et al., 1994; Merritts, 1996) (Figure 1), is a tectonically complex area that encompasses the onshore and offshore vicinity of Cape Mendocino. The MTJ forms a major tectonic transition from transform plate motion to the south, where the Pacific plate is moving in a northwest direction relative to the North America plate, to convergent plate motion to the north, where the plates are converging at an oblique angle with the denser, oceanic Gorda plate being subducted beneath the North America plate. The boundary between the Gorda plate to the north and Pacific plate to the south is the east-west trending Mendocino fault, a 260-km long right-lateral transform boundary that accommodates the motion of the Pacific plate relative to the motion of the Gorda plate (Bryant, 2001). Regional geological structures

associated with the tectonic forces acting at the MTJ are interpreted as forming over the past ~1 million years (Carver, 1992; Burger et al., 2002a).

Earthquakes and their impacts on the built environment are described using the concepts of either *magnitude* or *intensity*. Magnitude is a quantitative measurement of the amount of energy released by an earthquake at its source (USGS, 2020a). In this report we use the moment magnitude scale (here denoted as "M") to describe and compare different earthquakes based on magnitude. In comparison, intensity refers to how strongly shaking is felt at a location during an earthquake, and is described with the Modified Mercalli Intensity Scale (MMI) (USGS, 2020k) (Table 1). The MMI is divided into 10 levels (I-X) ranging from an MMI value of I (Not felt) to a value of X (Extreme). Because of the descriptive nature of the MMI, it is typically used for communicating information about earthquakes to non-scientists and communities in general or is used when little quantitative information is available. In contrast to earthquake magnitude, which is a single numerical value that describes the physical parameters of the earthquake, earthquake intensity varies and generally decreases with distance from the earthquake epicenter, although variabilities will occur based on substrate. Reports of intensity do not necessarily provide information about magnitude as intensity is not only dependent on distance from the earthquake source (hypocenter) but also on the site conditions (geologic material, building type, and site location such as in a valley versus ridgetop).

In the following sections we describe 5 seismic sources with the potential to generate intense and possibly long-duration shaking in onshore and offshore areas of the California North Coast. These sources are: (1) the southern end of the Cascadia subduction zone (CSZ); (2) the northern end of the San Andreas transform fault zone (SAF); (3) the Mendocino fault (MF); (4) the Gorda plate (GP); and (5) the fold and thrust belt of the accretionary wedge of the overriding North America plate, which underlies the coastal, nearshore and inland areas of Humboldt County. We describe sources of strong motion first in this review as other geological hazards that are important for the CalTrans SLR project (e.g., liquefaction, surface fault rupture and vertical land motion) may be driven, or triggered by seismic shaking or closely related to associated seismic source activity.

Table 1. The Modified Mercalli Intensity Scale (MMI).

Intensity	Shaking	Description/Damage
I	Not felt	Not felt except by a very few under especially favorable conditions.
II	Weak	Felt only by a few persons at rest,especially on upper floors of buildings.
III	Weak	Felt quite noticeably by persons indoors, especially on upper floors of buildings. Many people do not recognize it as an earthquake. Standing motor cars may rock slightly. Vibrations similar to the passing of a truck. Duration estimated.
IV	Light	Felt indoors by many, outdoors by few during the day. At night, some awakened. Dishes, windows, doors disturbed; walls make cracking sound. Sensation like heavy truck striking building. Standing motor cars rocked noticeably.
V	Moderate	Felt by nearly everyone; many awakened. Some dishes, windows broken. Unstable objects overturned. Pendulum clocks may stop.
VI	Strong	Felt by all, many frightened. Some heavy furniture moved; a few instances of fallen plaster. Damage slight.
VII	Very strong	Damage negligible in buildings of good design and construction; slight to moderate in well-built ordinary structures; considerable damage in poorly built or badly designed structures; some chimneys broken.
VIII	Severe	Damage slight in specially designed structures; considerable damage in ordinary substantial buildings with partial collapse. Damage great in poorly built structures. Fall of chimneys, factory stacks, columns, monuments, walls. Heavy furniture overturned.
IX	Violent	Damage considerable in specially designed structures; well-designed frame structures thrown out of plumb. Damage great in substantial buildings, with partial collapse. Buildings shifted off foundations.
X	Extreme	Some well-built wooden structures destroyed; most masonry and frame structures destroyed with foundations. Rails bent.

(USGS/Public Domain)

2 Potential Sources of Seismicity and Strong Shaking

2.1 Cascadia subduction zone (CSZ)

The Cascadia subduction zone (CSZ) consists of the megathrust (regional thrust fault) and associated deformation zone formed at the tectonic boundary between the subducting Juan de Fuca and Gorda plates and the overriding North America (PNSN, 2020) (Figures 1 and 2). The CSZ extends for approximately 1,300 km (800 mi) from northern California to Vancouver Island, B.C. (Zimmerman et al., 2005). The mapped location of the megathrust where it intersects the seafloor is at the western edge of the deformation front of the accretionary wedge (Personius and Nelson, 2006). This location increases in distance from shore from a few kilometers off northern California at Cape Mendocino to more than 100 km off Washington state at the Olympic Peninsula. At the southern extent of the CSZ, along the California North Coast, the megathrust dips landward about 10-15°, and separates the subducting mafic oceanic rocks and capping pelagic sediment of the Gorda plate from the Cretaceous, Miocene, and younger rocks of the overlying North American plate (McLaughlin et al., 2000).

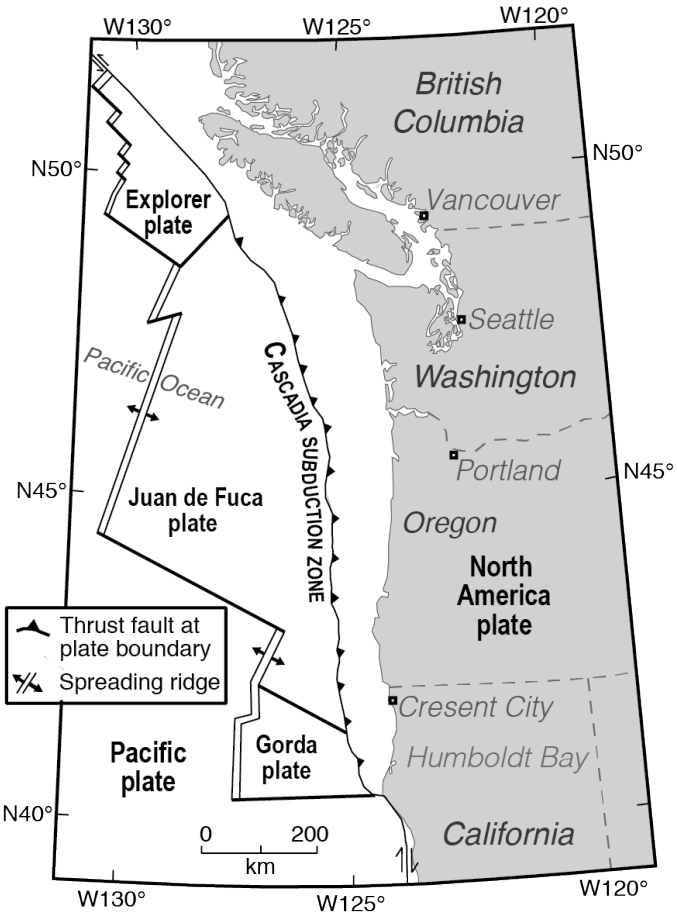

Figure 2. Map showing the extent of the Cascadia subduction zone off northwestern North America. This large tectonic boundary is the location of convergence of the Juan de Fuca and Gorda plates beneath the North America plate.

Subduction zones are the only sources on the earth capable of generating > M8.5 earthquakes (PNSN, 2020), as megathrusts may rupture along great distances, 100s of km, in a single event. Earthquakes of this magnitude generate strong shaking lasting for several minutes, a feature of earthquake behavior commensurate with the area (length and width) of the fault rupture (Wells and Coppersmith, 1994). Destructive tsunamis are commonly generated during subduction zone earthquakes as large volumes of seawater are displaced from sudden upheaval of the seafloor during fault rupture (Voit, 1987; Satake and Atwater, 2007; Sugawara et al., 2008), or from massive submarine landslides set in motion by the shaking (Watts, 2002; McAdoo and Watts, 2004; Didenkulova et al., 2010; Løvholt et al., 2015; Earthweb, 2020).

For example, the 1960 M9.5 southern Chile subduction zone earthquake, the largest ever recorded, ruptured over a distance of 1,000 km with subsequent shaking lasting 5-6 minutes, and produced a tsunami that impacted coastal sites around the Pacific Ocean (Plafker and Savage, 1970; Cifuentes, 1989; Fujii and Satake, 2013) (Table 2). The 1964 M9.2 Alaska earthquake ruptured 850 km of fault, with shaking lasting 4-5 minutes. A tsunami was generated from the megathrust rupture that propagated across the Pacific, causing loss of life and millions of dollars in damage to coastal infrastructure in Hawaii and the U.S. Pacific Northwest, including Crescent City in Northern California (Griffin, 1984; Lander et al., 1993). The 2011 M9.1 Tohoku-aki earthquake in Japan ruptured the megathrust over an area 500 km long and 200 km wide. Shaking lasted as long as 6 minutes and was felt across much of the island of Honshu (NASA, 2011). The height of the tsunami from this event was very well documented (Tsuji et al., 2014), with the measured variability of tsunami wave heights in the area of greatest impact shown to be correlated with local topography (Suppasri et al., 2011; Mori et al., 2011). On the Sanriku coast, the tsunami wave height averaged 20-30 m with a maximum of 40.5 m. Areas of low-lying coastal plain in the Miyagi and Fukushima prefectures were impacted by lower but still significant waves 10-20 m high.

Table 2. Example historical subduction zone earthquakes.

Subduction zone earthquake year and location	Magnitude (M)	Length of rupture (km)	Width of rupture zone (km)	Duration of shaking (minutes)	Tsunami average height / maximum height in area of greatest impact
1960 Chile	9.5	1,000	200	5-6	2-10 m / 25 m at Isla Mocha[1]
1964 Alaska	9.2	850	250	4-5	10-20 m / 32 m at Prince William Sound (Whittier, Chenega Cove)[2]
2004 Sumatra-Andaman	9.2	1,200	180	8-10	5-10 m / 50 m at Northern Sumatra[3]
2010 Chile	8.8	500	200	3	5-10/ 29 m at Maule region – Constitución[4]
2011 Tohoku-aki, Japan	9.1	500	200	6	20-30 / 40.5 m at Sanriku coast[5]

References for tsunami observations: 1–NCEI (2020); 2–Nicolsky (2013), Earthweb (2020); 3–Choi et al.(2006); 4–Fritz et al. (2011); 5–Suppasri et al. (2011).

The largest earthquakes emanating from the Cascadia subduction zone will be from sudden rupture and strain release along the megathrust, but significant earthquakes > M7 are possible from displacement of crustal faults within the overriding North America plate or faults deep within the subducting Gorda plate (USGS, 2020h). Like other subduction zones, the data show that the CSZ has and will rupture along segments of different lengths as well in full-margin ruptures (Nelson et al., 1995, 2006; Satake et al., 2003; Leonard et al., 2010; Goldfinger et al., 2012, 2013). Recent regional-scale modeling suggests large scale structural and lithological differences along the subduction zone north of California likely produce areas of smaller but significant earthquakes at times (Carbotte et al., 2024; Harrichhausen et al., 2024). Modeling suggests that these segment ruptures that only incorporate portions of the southern and central CSZ possess the potential to generate earthquakes in the range M7.4-8.7 (Goldfinger et al., 2013).

Prior to the1980s, the potential for the CSZ to produce great earthquakes was not well understood, because unlike other subduction zones fringing the Pacific, the CSZ had not ruptured in an M8 or larger earthquake during the more than 250 years since the arrival of European settlers on the northwestern

coast of North America and introduction of written history for the area. In addition, the subduction zone remains largely aseismic, another characteristic that is rare for active subduction zones globally. However, in the mid-1980s the potential for the CSZ to generate great earthquakes was revealed through breakthroughs in two areas of earthquake science: (1) geodetic and geophysical modeling that demonstrated the similarities between the CSZ and other subduction zones fringing the Pacific that produced major ruptures in the 20th century (Heaton and Kanamori, 1984; Heaton and Hartzell, 1986, 1987); and (2) a geological and geochronological study that provided field evidence for that great CSZ earthquakes had occurred in the past, and the approximate timing of those prehistorical events (Atwater, 1987).

The analyses by Heaton and Kanamori (1984) and Heaton and Hartzell (1986, 1987) showed that the CSZ had more characteristics in common with strongly coupled subduction zones that rupture in great (M8) to giant (M9) earthquakes than with "Marinas type, weakly coupled" (Heaton and Hartzell, 1987, p. 162) plate boundaries that do not produce large earthquakes. In particular they noted the similarities between convergence rate and age of the subducting slab at the CSZ with other subduction zones that had produced great historical ruptures: the 1960 M9.5 southern Chile subduction zone earthquake; the 1944 and 1946 M8.1 earthquakes off southwestern Japan; and the 1906 M8.8 earthquake in the northern Peru-Chile subduction zone off Columbia and Ecuador. The combination of high convergence rates, young and relatively buoyant subducting oceanic lithosphere, and amount of sediment supply at the megathrust interface of Cascadia compared to other seismogenic subduction zones suggest that the CSZ is capable of great earthquakes (Oleskevich et al., 1999).

The geophysical theories that the CSZ could produce great earthquakes were validated by Atwater (1987) who discovered geological field evidence for past subduction zone earthquakes and associated tsunami inundation in coastal southwestern Washington. The geological and chronological data at the type localities in Willapa Bay, Washington, showed evidence for 6 CSZ earthquakes in the past 3,500 years, some of which were associated with tsunamis. The stratigraphic signature of the past earthquakes discovered by Atwater (1987) adjacent to the CSZ is comparable to what is observed at coastal localities along other subduction zones such as Chile (Nelson et al., 2009; Garrett et al., 2015), Alaska (Savage and Plafker, 1991; Hamilton and Shennan, 2005; Shennan and Hamilton, 2006), and Japan (Imakiire and Koarai, 2012). It is characterized by marsh or forest soils showing evidence for abrupt burial by tidal flat mud, caused by land surfaces physically dropping relative to sea level during the earthquakes ("coseismic subsidence"), a result of the fault offset and flexure of the overriding plate during the subduction zone earthquake.

Since Atwater's (1987) seminal paper on field evidence for past CSZ earthquakes, scores of studies at coastal and estuarine sites along the length of the CSZ from California to maritime British Columbia have documented field evidence for CSZ earthquakes and worked to demonstrate earthquake correlation and recurrence among different sites. The accepted view now is that the CSZ has ruptured in >M8 earthquakes in the past and is currently locked by friction at depths shallower than about 30 km, building seismic stresses for a future rupture (Savage et al., 1991; Hyndman and Wang, 1995; Wang et al., 2003; Wang and Tréhu, 2016).

The most recent major CSZ earthquake occurred on 27 January 1700 C.E. It is interpreted as a >M9 full-margin rupture, and documented by field evidence along the length of the CSZ from California to British Columbia. The uniquely precise date of the 1700 C.E. earthquake, which preceded written history in maritime British Columbia and the U.S. Pacific Northwest, is based on historical records in Japan of a destructive tsunami that had no local source but was consistent with origins from a CSZ earthquake across the Pacific Ocean (Atwater et al., 2005). Using data on the inundation in Japan, Satake et al. (1996, 2003) were able to calculate both the date of the event and the amount of rupture (~M9) required to produce a tsunami of that size on Japan coast.

In northern California, investigations into the record of past CSZ earthquakes have focused on Humboldt Bay and the lower Eel River valley (Li, 1992; Carver et al., 1998; Patton, 2004; Pritchard, 2004; Engelhart et al., 2016; Hemphill-Haley, 2017; Padgett et al., 2021) and sites between the Klamath River and northern Crescent City (Abramson, 1998; Carver et al., 1998; Garrison-Laney, 1998; Peterson et al., 2011; Hemphill-Haley et al., 2019). Pertinent studies in central and southern Oregon include (Witter et al., 2001, 2003; Kelsey et al., 2002, 2005; Nelson et al., 2006; Hawkes et al., 2011; Goldfinger et al., 2012, 2013; Graehl et al., 2015; Peterson et al., 2015; Milker et al., 2016).

In southern Humboldt Bay, at Hookton Slough, Patton (2004) reported evidence for 4 past CSZ earthquakes, 2 of which may have been accompanied by tsunamis (Table 3**).**

Valentine et al. (2012) includes a compilation of stratigraphic, biostratigraphic, and radiocarbon data for sites between the lower Eel River valley and northern Humboldt Bay (Table 3). The earthquake chronology presented in this paper is based on unpublished masters theses and reports, in the 1980s and 1990s (Carver, 1992; Carver et al., 1998; Li, 1992; Valentine, 1992; Vick, 1988), and relies on bulk radiocarbon ages (Valentine et al., 2012, p. 1063) with the exception of 2 high-precision ages from other studies included to support findings for the 1700 C.E. event at upper Mad River slough: (1) a high-precision C14 age from the 1700 C.E. buried soil (Nelson et al., 1995) and a dendrochronological age from a tree stump (Jacoby et al., 1995). They conclude that these Humboldt Bay area data show deformation from 3-4 earthquakes from CSZ ruptures, and 2-3 earthquakes from local faults, in the past 2,000 years.

Recent work in northern Humboldt Bay provides the most updated evidence for the timing and amount of deformation (subsidence) from past CSZ earthquakes over the past ~1,700 years (Engelhart et al., 2016; Hemphill-Haley, 2017; Padgett et al., 2021, 2022) (Table 3). The shorter age range (~1,700 years) of the earthquake stratigraphy at northern Humboldt Bay sites is the result of a more recent development of tidally dominated marsh environments that are suitable for identifying earthquake stratigraphy.

Table 3. Ages and recurrence intervals of earthquakes for the past 3,000 years on the southern Cascadia subduction zone based on results of field studies between the lower Eel River valley and Crescent City, California.

Southern Humboldt Bay (Patton, 2004)	Humboldt Bay (Valentine, 2012)	Northern Humboldt Bay (Padjett et al., 2021	Crescent City and Lagoon Creek (Carver et al., 1988; Peterson et al., 2011)	Crescent City (Hemphill-Haley et al., 2019)
Radiocarbon ages of past CSZ earthquakes				
1700 C.E.[1]	1700 C.E.[1]	1700 C.E.[1]	1700 C.E.[1]*	1700 C.E.[1]*
–	–	875 cal yr B.P. (1075 C.E.)	943-743; 960-790 cal yr B.P. *	907-735 cal yr B.P.
-	1,400-1,150 cal yr BP	1,120 cal yr B.P. (830 C.E.)	1,055-778 cal yr B.P.*	–
1,696-1,522 cal yr B.P.*	1,650-1,500 cal yr BP[2]	1,620 cal yr B.P. (330 C.E.	1,690-1,350 cal yr B.P.*	~1,694-1,558 cal yr BP*
2,748-2,364 cal yr B.P.*	–	–	2,707-2,361 cal yr B.P.*	–
–	–	–	2,920-2,488 cal yr B.P.*	–
3401-3606 cal yr B.P.	–	–	–	–
Estimated recurrence for CSZ earthquakes				
650-720 yr (past 2,400 yr)	(no recurrence estimate provided)	245-625 yr (past 1,700 yr)	450 yr (past 3,000 yr)	(no recurrence estimate provided)
Ages of possible earthquakes on local faults				
–	500-600 cal yr BP	–	–	–
–	1,000-1,250 cal yr BP	–	–	–
–	1,900-1,750 cal yr BP	–	–	–

* Includes biostratigraphic evidence for tsunami inundation.

[1]Radiocarbon ages consistent with the full-rupture event in 1700 C.E.

[2]Valentine et al. (2012) questioned whether this event represented a local or regional event, but evidence for significant coseismic subsidence at Mad River slough and age overlap with a CSZ earthquake identified in northern Humboldt by Padgett et al. (2021) suggests it is likely a CSZ event.

The earthquake studies at Crescent City, Lagoon Creek, and Redwood Creek (Carver et al., 1998; Peterson et al., 2011; Hemphill-Haley et al., 2019) (Table 3**)** primarily rely on the presence of paleotsunami deposits to identify occurrences of past CSZ earthquakes, as the depositional environments mostly consist of freshwater marshes and lagoons where evidence for coseismic subsidence is less evident. However, Hemphill-Haley et al. (2019) identified both biostratigraphic and lithostratigraphic evidence for subsidence during the 1700 C.E. earthquake at Crescent City.

The long-term planning for the low-lying section of Hwy 101 adjacent to Arcata Bay will need to incorporate modeling that estimates the potential for strong motion and subsidence associated with CSZ megathrust events. The last ~M9 full-rupture earthquake on the CSZ occurred in 1700 C.E., and recurrence of great subduction zone earthquakes for the southern CSZ range from an estimated 245-720 years from the on-land record at Humboldt Bay and Crescent City (Table 2) to ~240 years from the offshore turbidite record (Goldfinger et al., 2012, 2013). Historical records of the intensity and duration of strong shaking from modern events of the past 50-60 years may be used as reliable analogs for effects on infrastructure from potential future events on the southern CSZ.

2.2 San Andreas fault (SAF)

The San Andreas fault (SAF) is part of a 100 km wide transform boundary that forms the interface between the Pacific and North America tectonic plates (Wallace, 1990; Schulz and Wallace, 1997). At this boundary, the Pacific plate is moving northwest relative to the North America plate, resulting in right-lateral offset across the fault. The entire SAF extends for about 1200 km (750 mi) from near the Salton Sea in southern California to the Mendocino triple junction offshore from Cape Mendocino in the north (Figures 1, 3**)**, and is divided into 3 sections (northern, central, and southern) based on different characteristics including slip rates and historical rupture history (Beeson et al., 2017; Berkeley Seismological Lab, 2020; Schulz and Wallace, 1997). The northern SAF, which extends from Hollister, California, in the south to the MTJ in the north, is the youngest section of the SAF. This section developed over approximately the past 10 million years by the northward migration of the triple junction (Wallace, 1990; Furlong and Schwartz, 2004; Stoffer, 2005), and experiences slip rates of about 35-40 mm/yr (Freymueller et al., 1999).

Potential strong shaking from earthquakes along the northern SAF is significant for the North Coast because of proximity and history of past events. The northern SAF has been the source of possibly 8-12 large earthquakes over the past few millennia based on paleoseismic research (Kelson et al., 2006; Niemi, 2010; Weldon et al., 2013; Zhang et al., 2006). Deep-sea turbidites can be generated by strong seismic shaking; their records are interpreted as recording two major ruptures of the northern SAF in the mid-1600s C.E. as well as ~1300 C.E. (Goldfinger et al., 2003). Within the last 200 years, there have been 3 significant ruptures along the northern SAF: the 1838 Peninsula San Andreas earthquake (~M7); the 1906 San Francisco earthquake (M7.9); and the 1989 Loma Prieta earthquake (M6.9) (Bakun and

Prescott, 1993; Ellsworth et al., 2013; Holzer, 1992; Schwartz et al., 2014; Streig et al., 2014; Toppozada and Borchardt, 1998).

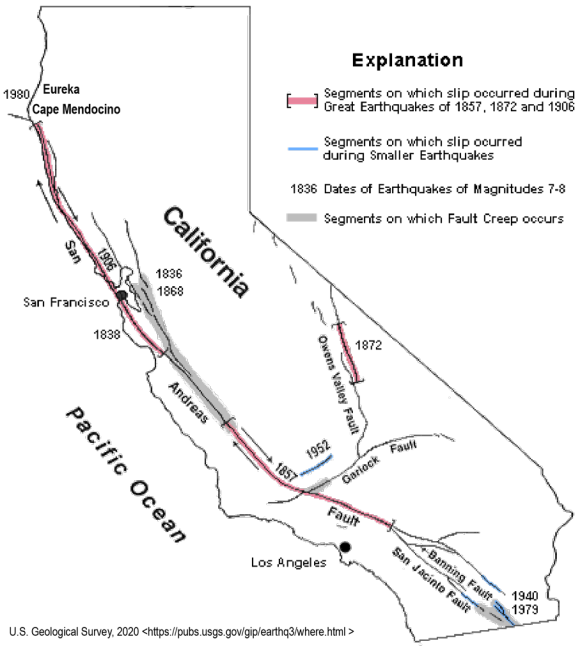

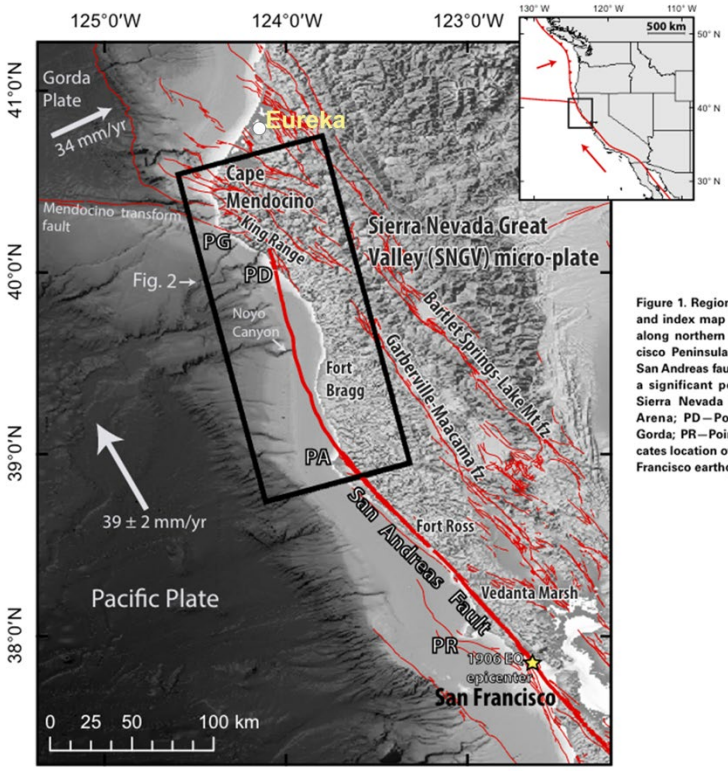

Figure 1. Regional digital elevation model and index map showing significant faults along northern California from San Francisco Peninsula to Cape Mendocino. The San Andreas fault zone (fz) accommodates a significant portion of North America–Sierra Nevada block motion. PA—Point Arena; PD—Point Delgada; PG—Punta Gorda; PR—Point Reyes. Yellow star indicates location of epicenter of the 1906 San Francisco earthquake.

Figure 3. The San Andreas fault. a) USGS base map of the San Andreas fault in California. The 1906 rupture extended from San Juan Batista in the south to off Cape Mendocino in the north (box indicates approximate area of 3b. b) northern extent of the San Andreas fault from recent high-resolution offshore seismic reflection and bathymetry showing the location of the reemergence of the fault at Shelter Cove (modified from Beeson et al., 2017).

The largest historical rupture for the northern SAF occurred on the morning of April 18, 1906. Based on historical accounts and reconstructions, its magnitude is estimated at M7.9 (Song et al., 2008). The epicenter of the earthquake was along a submarine section of the SAF west of San Francisco (Lomax, 2005; USGS, 2020g), but the fault ruptured bilaterally along the entire northern length of the northern SAF, from San Juan Bautista in the south to the Mendocino triple junction in the north, a distance of 477 km (296 mi) (Ellsworth et al., 2013; Prentice et al., 1999; Song et al., 2008; USGS, 2020j) (Figure 4). In comparison, the rupture length of the 1989 M6.9 Loma Prieta earthquake was about 40 km (25 mi) (USGS, 2020j). From historical accounts (Lawson and Reid, 1908; USGS, 2020j), strong shaking from the main shock persisted for 45-60 seconds, and shaking was reported as widely as southern Oregon to Southern California (Ellsworth et al., 2013; USGS, 2020j). Fault offsets varied along the length of the rupture, generally decreasing from north to south. The greatest offsets (8.6 m / 28 ft) were determined for the northernmost extent of the SAF at depth off Shelter Cove (Thatcher et al., 1997). At the surface, horizontal offset as great as 5 m (16.4 ft) was measured at Point Arena (Stover and Coffman, 1993, p. 114).

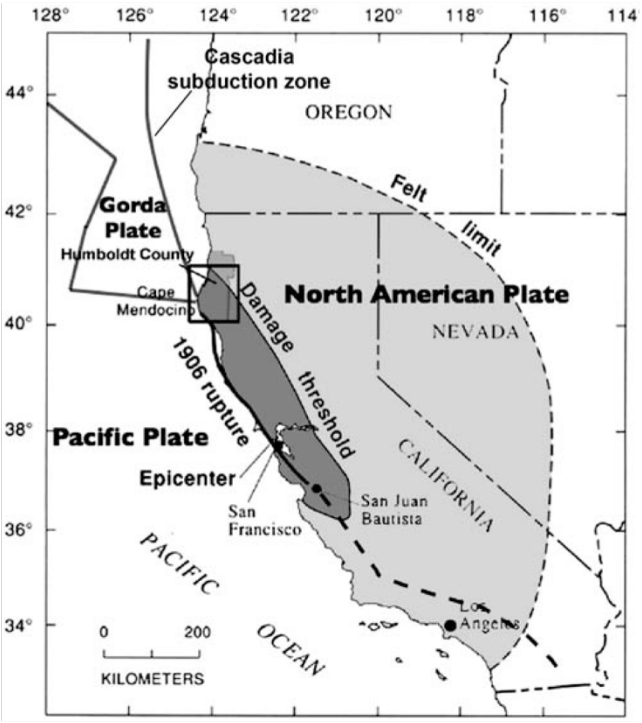

From Dengler et al., 2008, p. 919, figure 1.

Figure 4. Map showing the 1906 rupture length of the San Andreas fault and area of impact from the earthquake.

Shaking intensity on the MMI scale for the North Coast ranged from VI-VIII for the Eureka area; the Petrolia/Mattole area experienced even greater MMI levels of VIII-IX (Figure 5) (Boatwright and Bundock, 2005; Dengler, 2008; USGS, 2020g). The high MMI values so far from the epicenter of the earthquake are consistent with the greatest fault offsets occurring at the north end of the fault off Shelter Cove (Thatcher et al., 1997; Prentice et al., 1999; Boatwright and Bundock, 2005; Dengler, 2008; Song et al., 2008).

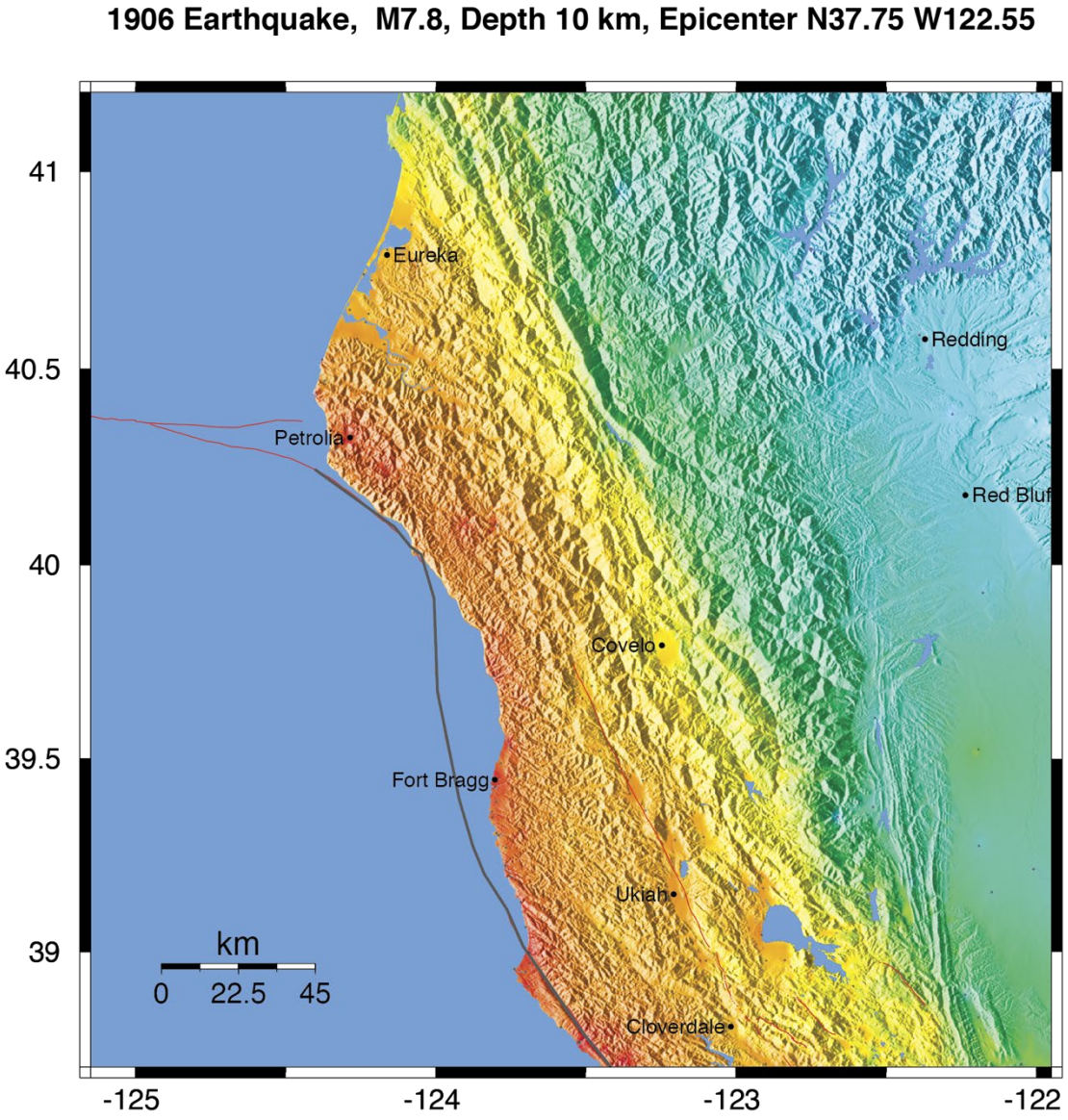

PERCEIVED SHAKING	Not felt	Weak	Light	Moderate	Strong	Very strong	Severe	Violent	Extreme
POTENTIAL DAMAGE	none	none	none	Very light	Light	Moderate	Moderate/Heavy	Heavy	Very Heavy
PEAK ACC.(%g)	*<.17*	*.17-1.4*	*1.4-3.9*	*3.9-9.2*	*9.2-18*	18-34	34-65	65-124	>124
PEAK VEL.(cm/s)	<0.1	0.1-1.1	1.1-3.4	3.4-8.1	8.1-16	*16-31*	*31-60*	*60-116*	*>116*
INSTRUMENTAL INTENSITY	I	II-III	IV	V	VI	VII	VIII	IX	X+

From Boatwright and Bundock, 2005 <https://pubs.usgs.gov/of/2005/1135/IntensityMaps.html>

Figure 5. Modified Mercalli Intensity shake map of northern California for the 1906 San Andreas fault earthquake.

Damage to structures in Humboldt County from shaking and liquefaction was extensive for various communities proximal to Humboldt Bay and otherwise, including areas of southern Humboldt County and the community of Ferndale (Dengler, 2008; Youd & Hoose, 1978). According to Dengler (2008 p. 819), accelerations and areas of strong shaking from the 1906 San Francisco earthquake likely exceeded those of the 1992 M7.2 Cape Mendocino earthquake and in fact "based on the severity of damage and scale of liquefaction, the 1906 earthquake was Humboldt County's strongest historic event.

Youd and Hoose (1978, pp. 170–173) compiled historical records of damage in Humboldt County, which among other listings included:

- liquefaction and lateral spreading all along the Eel River at Dungan's Ferry (p. 170)
- decommissioning of the Scotia Railroad because of a large landslide on the Eel River and damage to metal beams on the railroad bridge (p. 171)
- major liquefaction and lateral spreading at Cock Robin Island and Cannibal Island near Ferndale, with 1-10 ft of subsidence from liquefaction and numerous sand boils present (p. 171)
- damage to chimneys across communities south of Eureka (p. 171)
- 100 ft long fissure in road at Field's Landing (p. 171)
- subsidence and damage at Pelican Island across from Field's Landing such that the US Pile Beacon dropped by 3 ft and was left standing at a 45° angle (p. 171)
- Sand boils and deep cracks from lateral spreading at Field's Landing (p. 172)
- Water mains for the Eureka Water Company broken by subsidence at Elk River (p. 172)
- pipes and roads cracked at place called Sweasy Ranch near Eureka (p. 172)
- land around the Eureka foundry cracked and subsided (p. 172)
- water mains of the Eureka Water Company were twisted and broken as the ground heaved up (p. 172)
- ground subsidence (from liquefaction) of several feet beneath the Vance Company mill and warehouses in Samoa (p. 173)
- subsidence in marshy areas (from liquefaction) between Eureka and Arcata (p. 173)
- cave-in at one end of the Loleta train tunnel (p. 173)

Long term planning for the Hwy 101 project between Eureka and Arcata will need to consider probabilities of large earthquakes along the northern SAF. The recurrence interval for earthquakes on the northern SAF that are large enough to generate offsets that can be measured in the geologic record is about 200 years (Field et al., 2014; Schwartz et al., 2014; Weldon et al., 2013). The probability for a 1906-size event to occur within the planned project time of the project portion of Hwy 101 will need to be investigated. Field et al. (2014) report a 30% probability that the San Francisco Bay Area will experience a M7.5 earthquake in the next 30 years, but note that rupture is more likely along faults within the San Andreas fault zone to the east of the SAF, namely the Hayward-Rodgers Creek and Calaveras Faults, which have not ruptured as recently as the 1906 northern SAF event (Field et al., 2014; Watt et al., 2016). How rupture along these faults and their northern extensions will affect the

Humboldt Bay area will need to be evaluated. Petersen et al. (2020) and Rukstales and Shumway (2019) provide probabilistic estimates for strong motion within the continental US. They estimate that the northern coast of California has a 10% chance of peak horizontal ground accelerations exceeding 0.4 to 0.8 g in 50 years (Figure 6).

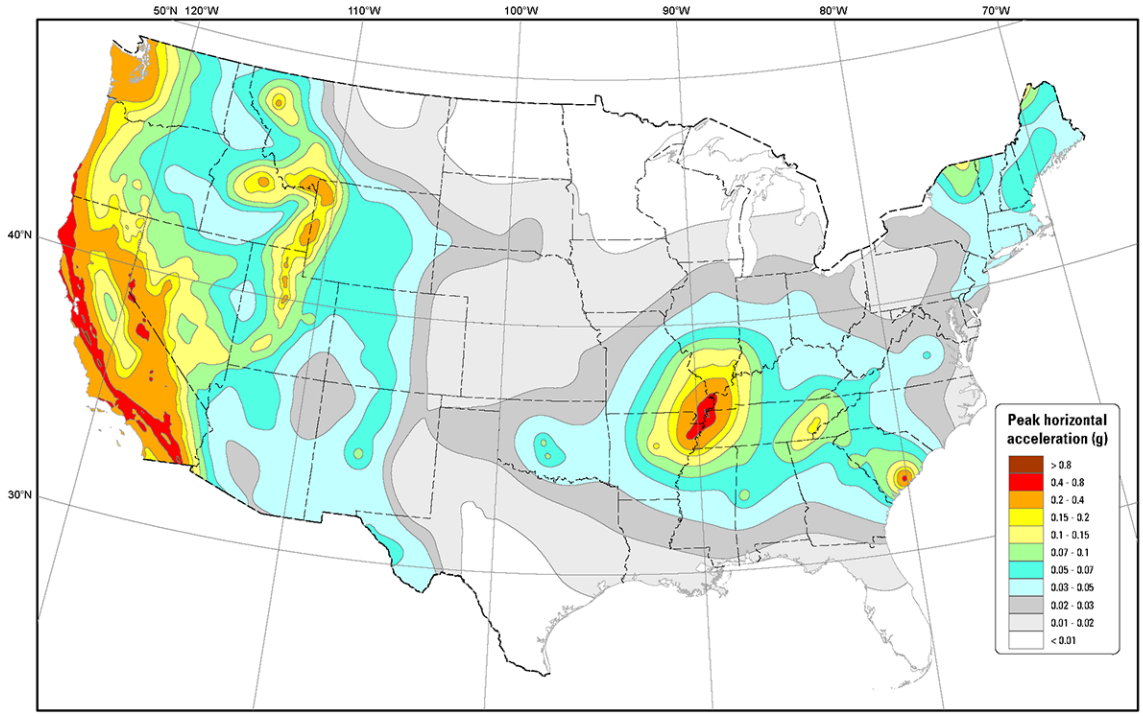

Figure 6. Probabilistic seismic hazard model showing a 10% probability of peak ground accelerations exceeded 0.4-0.8 g in coastal Northern California over the next 50 years. (From Rukstales and Shumway, 2019, < https://www.sciencebase.gov/catalog/item/5d5597d0e4b01d82ce8e3ff1>.

2.3 Mendocino Fault (MF)

The Mendocino fault (MF) is a near-vertical, right-lateral and reverse transform boundary that separates the Pacific plate to the south and Gorda plate to the north (Figure 1). The MF strikes east-west for about 260 km (160 mi) from the MTJ to the Gorda Ridge near longitude 127.5°W (Bryant, 2001; Dengler et al., 1995). The divergent spreading at Gorda Ridge is driven by the right-lateral motion along the MF (McLaughlin et al., 2000).

The Mendocino fault is a high seismicity region and a frequent source of felt seismic shocks for the North Coast (Bryant, 2001), although most earthquakes generated in this area are small. A search of the USGS interactive online earthquake map (https://earthquake.usgs.gov/earthquakes) shows > 400 earthquakes greater than M4.5 along the MF since 1960, and 63 that exceeded M5. However, only

earthquakes at the eastern end of the MF will likely impact onshore and nearshore infrastructure. For example, the 1994 M6.9 earthquake on the MF, although a large event, was 140 km (85 mi) from shore. Intensities did not exceed MMI-III on land and it caused little damage (Dengler et al., 1995). Larger and closer events on the MF are possible, however, according to Bakun (2000) who estimated from historical records that a possible M7 earthquake occurred on the MF in 1878 within 75 km (46 mi) from shore.

Further discussion on recent (post-1960) earthquakes along the MF is provided in Section 3.3 ("North Coast Earthquakes > M6.0 Since 1960").

2.4 Gorda plate

The Gorda plate encompasses the southernmost oceanic tectonic plate being subducted beneath the North America plate at the Cascadia subduction zone (Figure 1). It extends between about latitudes 40°N and 43°N and is separated from the Juan de Fuca plate to the north by the Blanco fracture zone (Figures 2, 7; Table 4). Earlier studies included the Gorda plate as a southern section of the Juan de Fuca plate (e.g., Dziak et al., 2001; Rollins and Stein, 2010; Stoddard, 1991), but it is now recognized as a distinct tectonic plate with characteristics different from either the Juan de Fuca plate to the north or Pacific plate to the south of the MF and MTJ (Chaytor et al., 2004; Dziak et al., 2001; Fox and Dziak, 1999; Gulick et al., 2001).

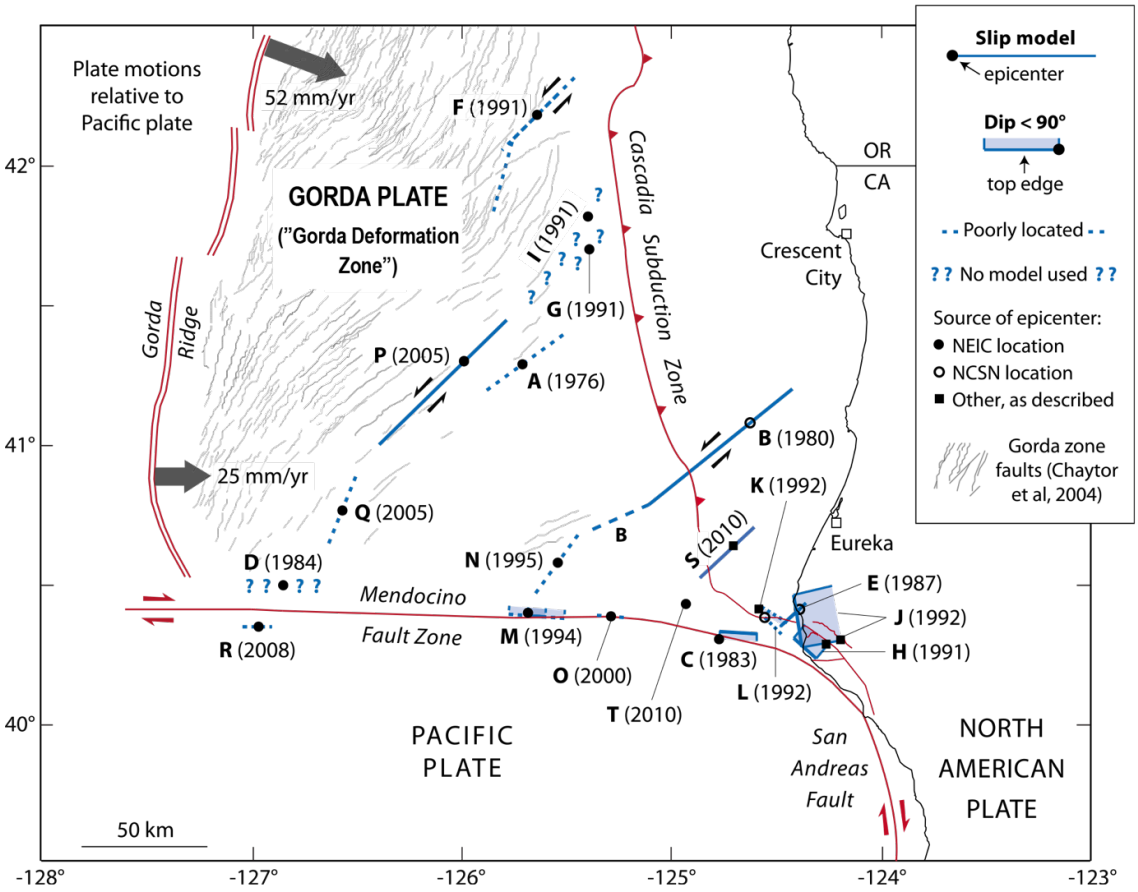

Figure 7. Map of the Gorda plate ("Gorda deformation zone") by Rollins and Stein, 2010. Letters indicate epicenters for earthquakes > M5.9 between the years 1976 and 2010. Earthquake magnitudes are listed in Table 4.

Table 4. Earthquakes shown on Figure 7, the Rollins and Stein (2010) map of the Gorda plate ("Gorda deformation zone"). Earthquakes shown are those >M5.9 that occurred during the time period 1976-2010.

Epicenter ID shown on Figure 7	Year	Magnitude (M)	Earthquake epicenter ID shown on Figure 7	Year	Magnitude (M)
A	1976	6.7	K	1992	6.5
B	1980	7.3	L	1992	6.6
C	1983	6.1	M	1994	7.0
D	1984	6.6	N	1995	6.6
E	1987	6.0	O	2000	5.9
F	1991	6.8	P	2005	7.2
G	1991	6.3	Q	2005	6.6
H	1991	6.1	R	2008	5.9
I	1991	7.1	S	2010	6.5
J	1992	6.9	T	2010	5.9

Data summarized from Rollins and Stein, 2010, p. 3, Table 1

The Gorda plate is actively deforming under tectonic stresses and therefore an area of frequent fault rupture and seismicity (Tobin and Sykes, 1968; Kilbourne and Saucedo, 1981; Wilson, 1989; Fox and Dziak, 1999; Gulick et al., 2001; Dziak et al., 2001; Chaytor et al., 2004; Rollins and Stein, 2010). It is also the primary source of felt earthquakes for the North Coast area (USGS, 2020i).

A prominent feature of the Gorda plate area is the preponderance of northeast striking left-lateral faults (Stoddard, 1991; Smith et al., 1993; Gulick et al., 2001; Chaytor et al., 2004; Wilson, 2012) (Figure 7, Table 4). This faulting pattern is the result of the north-south compression and east-west extension that the Gorda plate experiences because of its position between the subducting Juan de Fuca plate to the north and the east-west striking Mendocino fault to the south (Rollins and Stein, 2010). In addition, the Gorda plate as a mass is rotating in a clockwise direction as it concurrently moves eastward toward the subduction interface, a result of slower spreading rates in the southern part of the Gorda Ridge compared to the north, compiling the tectonic stresses and propensity for brittle deformation (Wilson, 2012) (Figure 7).

The geologically frequent, earthquake-generating, left-lateral fault ruptures (intra-slab) in the Gorda plate are the result of the combined tectonic forces of compression, extension, and internal plate rotation. (Figure 7). As described by Rollins and Stein (2010, p. 1), the Gorda plate[1] is "*a 50,000 km^2 area of diffuse shear and rotation offshore northernmost California*" which "*has been the site of 20 M ≥ 5.9*

[1] Rollins and Stein (2010) referred to the Gorda plate as the "Gorda deformation zone."

earthquakes on four different fault orientations since 1976, including four M ≥ 7 shocks." Rollins and Stein (2010, p. 1) noted that, based on the frequency and size of earthquakes, the Gorda plate produced "*the highest rate of large earthquakes in the contiguous United States*." In addition to the 20 earthquakes between 1976-2010 described by Rollins and Stein (2010) (Figure 7, Table 4), an additional 5 earthquakes > M5.9 have been recorded from the Gorda plate: an M6.5 event in 2010; an M6.8 event in 2014; an M6.6 event in 2016; a M6.2 event in 2021; and an M6.4 event in 2022 (USGS, 2020i; Yeck et al., 2023; Yoon and Shelly, 2024). Wong (2005) proposed that north of the Cape Blanco fracture zone, thermal and tectonic processes of the Juan de Fuca plate make it distinctly different seismically and nearly incapable of producing large intra-slab earthquakes. The issue of frequent seismicity in the Gorda plate is examined further in Section 3.0, below.

The Gorda plate is seismically active and is the tectonic plate adjacent to, and subducting beneath, the North Coast. Future considerations of the Hwy 101 project will have to consider the shaking effects of fault rupture in the Gorda plate, potentially within close enough proximity to the highway to represent a major seismic hazard. It is unlikely that a Gorda Plate event will be directly responsible for tectonic surface rupture in the project area.

2.5 Faults in the Fold and Thrust Belt of the Accretionary Wedge

The Cascadia subduction zone accretionary prism in the North Coast area is an approximately 85 to 100 km wide and 2,500 m thick zone of sedimentary rocks consisting of deformed deep-trench and lower-slope Miocene basin sediments overlain by the shallower water "Wildcat Group" consisting of late Pliocene to Pleistocene shelf and margin deposits (Ogle, 1953; Field et al., 1980; Woodward-Clyde Consultants, 1980; Clarke and Carver, 1992; Swan et al., 2002; Hill et al., 2020). These sedimentary units, in turn, overlie middle Jurassic to early Tertiary Franciscan Complex metasedimentary and igneous rocks (Ogle, 1953; Burger et al., 2002b). The dominant feature of the accretionary prism is the approximately 210 km long Eel River basin, a forearc basin, bordered on the west by the subduction zone (Figure 8). The basin extends from north of Cape Mendocino where, onshore, it comprises the northwest trending Eel River valley; offshore it becomes north-northwest oriented and extends to near Cape Sebastian, Oregon (Burger et al., 2002b).

Faults and folds that are part of the upper-plate structure of the Cascadia subduction margin have been identified in bathymetric and seismic sections within the accretionary prism (Figures 8, 9, and 10), with evidence that they have deformed or offset basin-fill deposits, and some instances, Holocene marine sediments (Field et al., 1980; Woodward-Clyde Consultants, 1980; Clarke and Carver, 1992; McLaughlin et al., 2000; Swan et al., 2002; Burger et al., 2002b; Hill et al., 2020). Clarke and Carver (1992) and McLaughlin et al. (2000) define the faults as southwest-vergent (hanging wall moving toward the southwest), northeast-dipping thrust faults that create imbricated faulted sections of the marine sediments. Associated with the thrust faults are asymmetric, hanging-wall folds that form synclinal troughs and anticlinal ridges. Field et al. (1980) describe the offshore structures as "broad and gentle to narrow and tight; most are symmetrical or nearly so." Clarke and Carver (1992) and McLaughlin et al. (2000) note that sediments are more intensely deformed at the southern end of the accretionary prism,

likely as a result of stronger coupling as the Cascadia megathrust encounters the Mendocino fault and comes closer to land. Field et al. (1980) describe relief across the surface of the accretionary prism to be up to 200 m as a result of folding of sediments as young as Holocene in age. Both the Little Salmon and Table Bluff faults, which are the closest to the offshore megathrust, are represented in the bathymetry and in subsurface seismic sections shown in Figures 9 and 10. These faults may be considered as analogs to the Fickle Hill fault which is located farther north and is part of the Mad River fault zone.

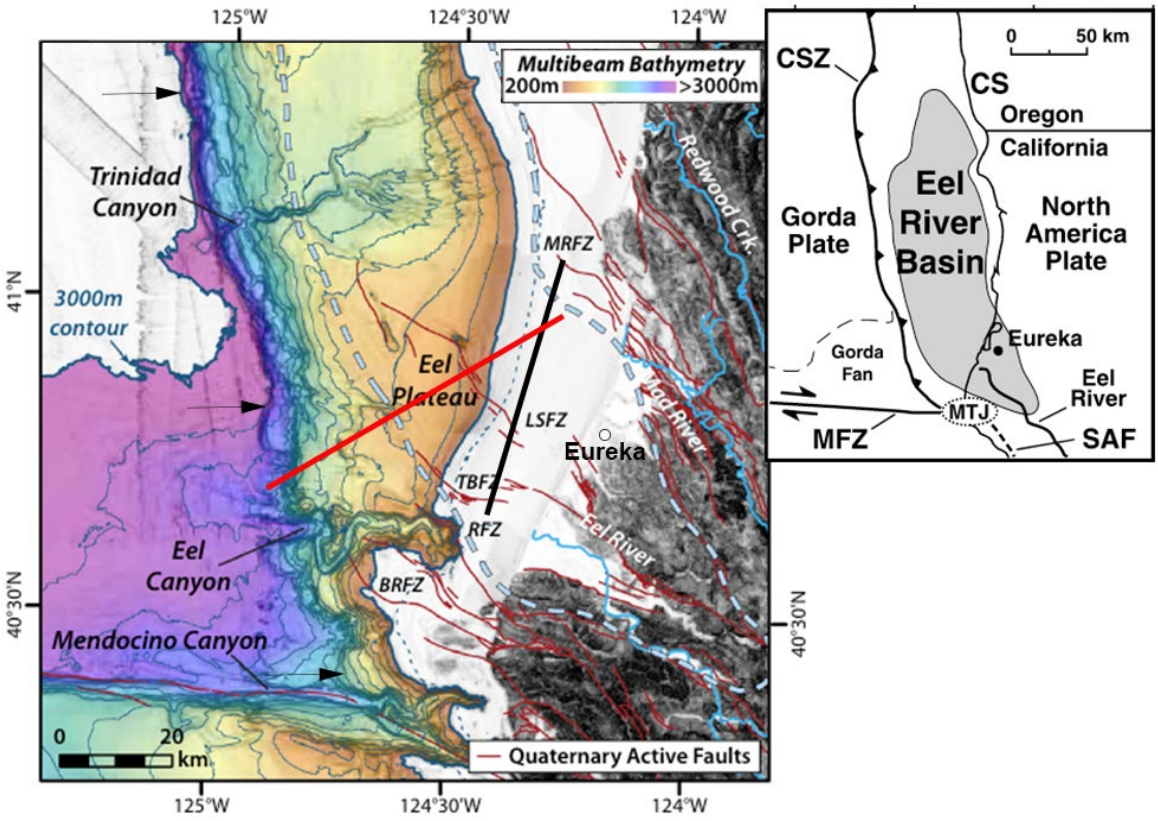

Figure 8. A portion of the Cascadia subduction zone accretionary prism with bathymetry offshore of Eureka (open white circle). The colored bathymetric area is limited to water depths greater than 200 m. Heavy blue dashed line represents the borders of the Eel River forearc basin which lies immediately east of the subduction zone (see inset for full extent of the basin parallel to the subduction zone (modified from Burger, et al., 2002). Bold black line represents approximate location of seismic reflection profile in Figure 9 from Burger et al., 2002). Bright red solid line is approximate location of seismic profile perpendicular to the accretionary prism and trench (from Hill et al., 2020). Dark red lines are Quaternary active faults. Black arrows indicate location of the Cascadia subduction zone trench and the upward approximate location of the megathrust. The accretionary prism extends onshore as well (Modified from Hill et al., 2020, their Figure 3).

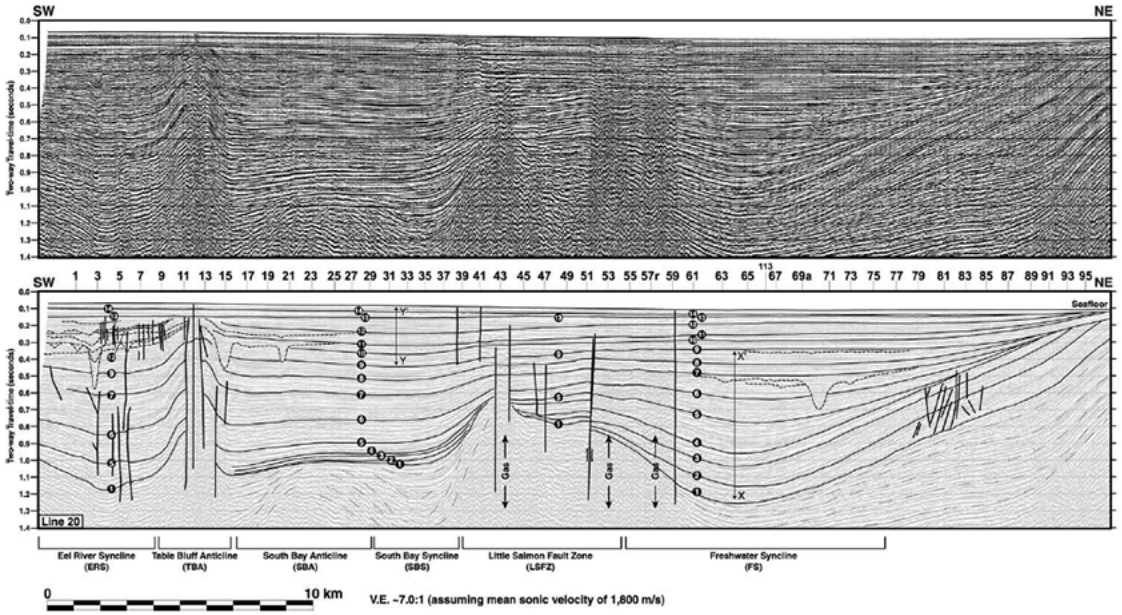

Figure 9. Uninterpreted and interpreted seismic reflection profile constructed in NE to SW azimuth roughly parallel to the coastline (See Figure 8 for location). Profile shows Freshwater, South Bay and Eel River synclines (associated with Arcata Bay, South Bay and Eel River Valley, respectively), Little Salmon South Bay and Table Bluff anticlines as well as faults within the Little Salmon and Table Bluff fault zones. Interpretations represent faults as nearly vertical structures which is great contrast to on land documentation of faults dipping at between 20°-35°. Several faults within each zone are interpreted to displace youngest sediments. (From Burger et al., 2002, their Figure 3).

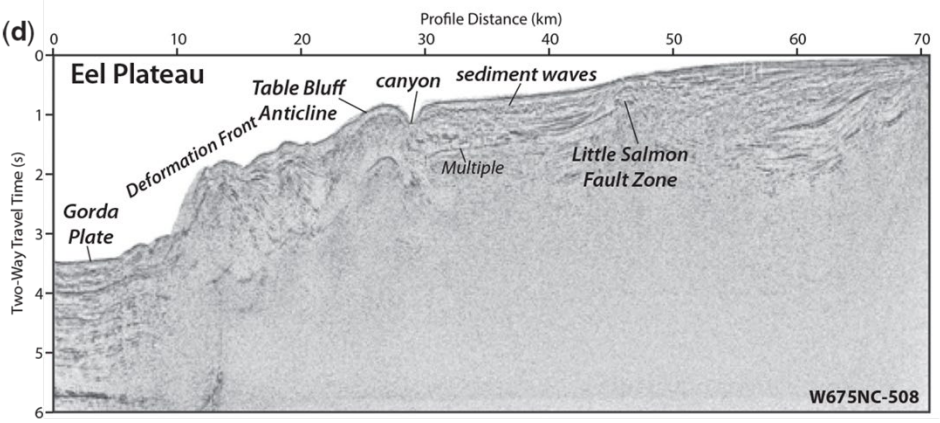

Figure 10. Multi-channel seismic profile constructed in a NE-SW azimuth immediately offshore of Humboldt Bay (see Figure 8 for profile location). Of note are the oceanic Gorda plate to the west, the steep, highly deformed, deformation front at the seaward end of the Cascadia megathrust, and the Table Bluff and Little Salmon anticlines (and associated faults). (From Hill et al., 2020, their Figure 6d).

Swan (2002) describes a series of onshore Quaternary anticlines (Figure 11) as active thrust fault-associated folds that are the projection of related structures identified offshore (Field et al., 1980; Clarke and Carver, 1992; Burger et al., 2002a; Hill et al., 2020). These include the Table Bluff anticline and Humboldt Hill (also referred to as the Little Salmon anticline) as well as the Mad River fault zone which includes active faults within the northern part of the project area and include, from north to south, the Fickle Hill fault and smaller faults such as Bayside, Bracut and Freshwater faults, respectively (Figure 11).

These folds have up to 1.5 km of structural relief and are asymmetrical. Faults within the Mad River fault zone dip northeastward. Swan (2002) also describes a series of subsiding, synclinal basins in the onshore area that include the Freshwater syncline forming Arcata Bay and the South Bay syncline that forms Southern Humboldt Bay (Figure 12). Although the seismic section depicted in this figure does not extend northward through the project area, evidence suggests a similar structural architecture through Arcata Bay.

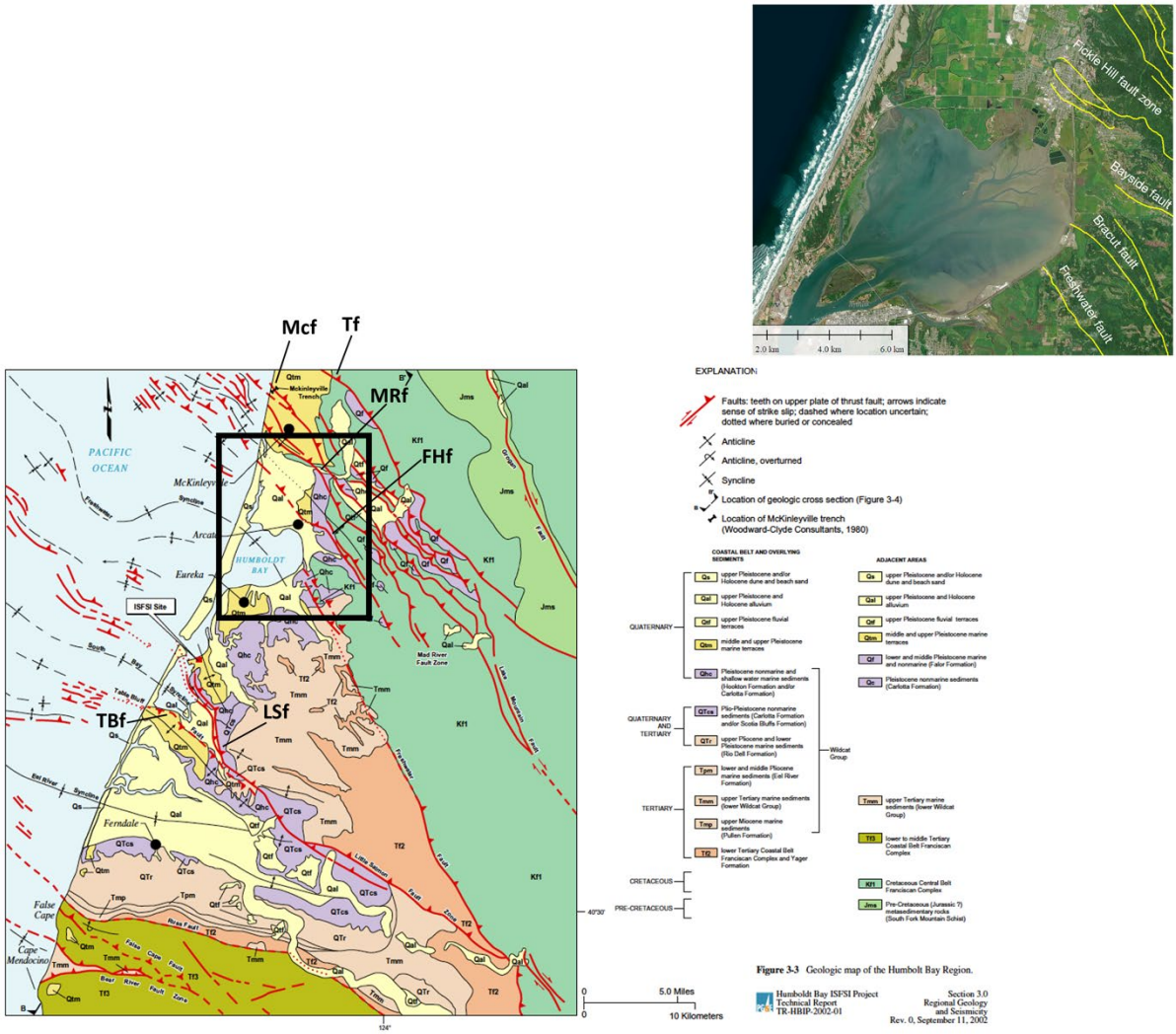

Figure 11. Geologic map of the Humboldt Bay Region. Of special note are the locations of the Eel River, South Bay, and Freshwater synclines and the Table Bluff (TBf), Little Salmon (LSf) (in the South Bay) and Mad River fault zone (Trinidad fault (Tf), McKinleyville fault (McF), Mad River fault (MRf), and Fickle Hill fault (FHf) north of Arcata Bay. Box represents inset image that shows details of the northern Arcata Bay including the Fickle Hill, Bayside, Bracut and Freshwater faults). These faults extend offshore and are part of the Cascadia accretionary prism. (Geologic map from Swan, 2002, his Figure 3.3).

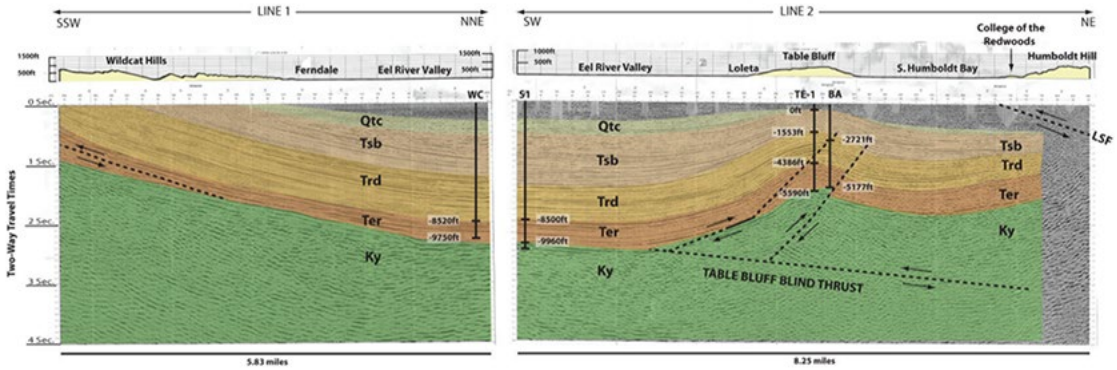

Figure 12. Interpretation of proprietary seismic section from SSW to NE across the Eel River basin, Table Bluff anticline and Humboldt Hill. The main Table Bluff fault is interpreted to be a north-dipping, blind thrust fault, with the Table Bluff anticline representing the surface expression of a south-dipping backthrust fault. The Little Salmon fault is thrusting Humboldt Hill southward over Tertiary and younger sediments to the south. (From Vadurro, 2006, his Figure 3).

2.5.1 Little Salmon Fault

The Little Salmon fault is a major component of the upper plate fold and thrust belt structures of the Cascadia subduction zone. It has been described as the southern 95 km of a 330 km long collection of active faults and folds referred to as the Little Salmon fault system (Swan et al., 2002). Onshore, the fault zone extends from the south, near Bridgeville, California, and strikes northwest along the Van Duzen river valley through Humboldt Bay (Woodward-Clyde Consultants, 1980; Kelsey and Carver, 1988a; Swan et al., 2002; Nicovich, 2015). From there it continues offshore striking northwest as far as offshore southern Oregon (Swan, 2002). The offshore portion of the fault zone parallels the Cascadia subduction deformation front in a system of *en echelon* anticlines and thrust faults (Swan et al., 2002). Burger et al. (2002) image the Little Salmon fault as an approximately 7.5 km wide broad anticline associated with near vertical faults. The on-land, upper portion of the fault dips to the northeast at about 20° to 35° (Woodward-Clyde Consultants, 1980; Kelsey and Carver, 1988b; McCrory, 2000). On land it is described as 20 to 25 km wide, extending south to north from the Table Bluff anticline to the Freshwater syncline (Swan et al., 2002).

Terrestrial fault studies define the Little Salmon fault zone as consisting of imbricate, south-vergent thrust sheets consisting of at least three splays at Humboldt Hill, which is an associated active hanging wall anticline. These splays are interpreted as active during the Holocene (Swan, 2002; Vadurro et al., 2006; Woodward-Clyde Consultants, 1980). The southwestern most splay has been identified as having the greatest Holocene displacement (Carver & Burke, 1988; Swan, 2002; Witter et al., 2002; Woodward-Clyde Consultants, 1980). This splay is located along the margin of Humboldt Bay at the southwestern base of Humboldt Hill (Figure 11). The middle splay of the fault has been documented through the College of the Redwoods campus by the consulting firm LACO Associates (Vadurro et al., 2006). At that location the deformation is displayed as a single, low angle, northeast-dipping thrust fault with a complex series of hanging wall backthrusts, normal faults, and folds that span a distance of more than 500 m.

The eastern trace of the fault lies within the lower slopes of Humboldt Hill, traverses the upper, eastern part of the College of the Redwoods campus and extends northwestward where it passes immediately south of Buhne Point and the PG&E power plant site, where it is referred to as the Bay Entrance fault (Swan et al., 2002). Proprietary deep seismic survey data (Figure 12) provide a suggestion that the Little Salmon fault and adjacent Table Bluff fault sole into the Cascadia megathrust at depth (Swan, 2002).

Paleoseismic investigations of the onland portion of the fault indicate at least 3 surface rupture (coseismic) events in the last 1,700 to 2,000 years with individual slip events accounting for 1 to more than 4 m of displacement. (Carver and Burke, 1988; Swan et al., 2002; Witter et al., 2002). Using empirical relations for 80 global earthquakes between maximum displacement and magnitude (Wells and Coppersmith, 1994) we can estimate that the earthquakes associated with these displacements at a minimum are between M6.7 and 7.1. The most recent event occurred about 300 years ago. There is suggestion, but not definitive evidence, that movement of the Little Salmon fault may be coincident with at least some Cascadia megathrust events but not the most recent subduction zone event which occurred in 1700. Although there is no direct surface rupture hazard from this fault at the project site, we recognize it to likely be the most active of the fold and thrust belt faults which could produce strong ground motion at the site.

2.5.2 Mad River fault zone

The Mad River fault zone (Figure 11), from north to south, includes the Trinidad, Blue Lake, McKinleyville, Mad River, Fickle Hill, Bayside, Bracut and Freshwater faults (Woodward-Clyde Consultants, 1980; McCrory, 1996, 2000; Pacific Gas and Electric Company, 2002, 2017; Padgett, 2019; Padgett et al., 2019). Studies of activity and slip rate have been conducted on some but not all faults within this zone. To date, little is known about the Freshwater, Bracut or Bayside faults except for their associations with the Freshwater Syncline and nearby Fickle Hill fault (Figure 11). Faults within the majority of faults within the Mad River fault zone strike northwest and dip between 25 and 45° NE (Woodward-Clyde Consultants, 1980; Carver and Burke, 1988; McCrory, 2000). Although the faults within the northern portion of the Mad River fault zone (i.e., Trinidad, Blue Lake, McKinleyville and Mad River) are considered active and potential seismic sources, this evaluation will discuss those faults closer to the project area. McCrory (2000) reports fault lengths within the zone to range from 26 – 40 km (16 – 25 mi) onshore and extend an additional 20 – 50 km (12.4 – 31 mi) offshore. Using empirical relations between earthquake surface rupture length and magnitude (Wells and Coppersmith, 1994), the onshore portion of these faults, if they rupture their entire lengths could produce earthquakes ranging from approximately M6.5 to 6.8. The associated surface rupture displacements may be in excess of 1 m in the form of folding and surface scarps.

Fickle Hill fault

McCrory (1996, 2000) describes the Fickle hill fault as a N40°W-striking, 25° NE southwest-vergent thrust fault. It is located along the southwestern base of and within the hillside of Fickle Hill (Figure 11). It strikes NW-ward where it traverses the city of Arcata within 3 prominent splays. Activity of the fault is

based largely on displacement of late Pleistocene marine terrace treads (ca. 83 ka reported by Carver and Burke (1988). Kelsey and Carver (1988) report a slip rate of up to 1 ± 0.2 mm/yr for the fault.

3 North Coast Earthquakes >M6 Since 1960

The proximity of the California North Coast to the complex tectonic regime of the Mendocino triple junction and the deforming Gorda plate make it the most seismically active region in the conterminous United States.

Since the mid-1960s, seismicity in Central and Northern California has been closely monitored through the Northern California Seismic System (NCSS, 2020), a collaborative effort between the U.C. Berkeley Seismological Laboratory and USGS. Since the launch of the NCSS, thousands of earthquakes have been recorded in the North Coast region (USGS, 2020i), the vast majority of which were too small to be detected except by seismographic instruments, or were felt by local citizens but did not result in damage to infrastructure. For example, a search for recorded seismicity in an area bounded by latitudes 39°-43°N and longitudes 128°-123°W—which encompasses the North Coast region and NCOWS area—identified almost 4,000 earthquakes > M2.5 in the past 24 years (2000-2024) (Figure 13) (USGS, 2020i). In comparison, the area to the north encompassing the next 4 degrees of latitude (43°-47°N) recorded 669 earthquakes >M2.5 over the same time period. In the area encompassing 4-degrees of latitude farther to the south, between 35°-39°N, there were 56 earthquakes > M2.5 during this time.

These data show that the North Coast region experiences exceptionally frequent seismicity, higher than compared to any other area of the conterminous U.S. And although most of the seismicity is associated with low-magnitude earthquakes, the area has experienced 20 significant earthquakes > M6 associated with deformation of the Gorda plate and Mendocino fault in just the past 64 years (Figure 14, Table 5). Earthquakes within the Gorda plate are the result of fault rupture both westward of the subduction interface and to the east along the extent of where the oceanic Gorda plate is being subducted beneath the North American plate. This complex series of ruptures within the Gorda plate occur on numerous faults that are poorly mapped and understood (Figure 7).

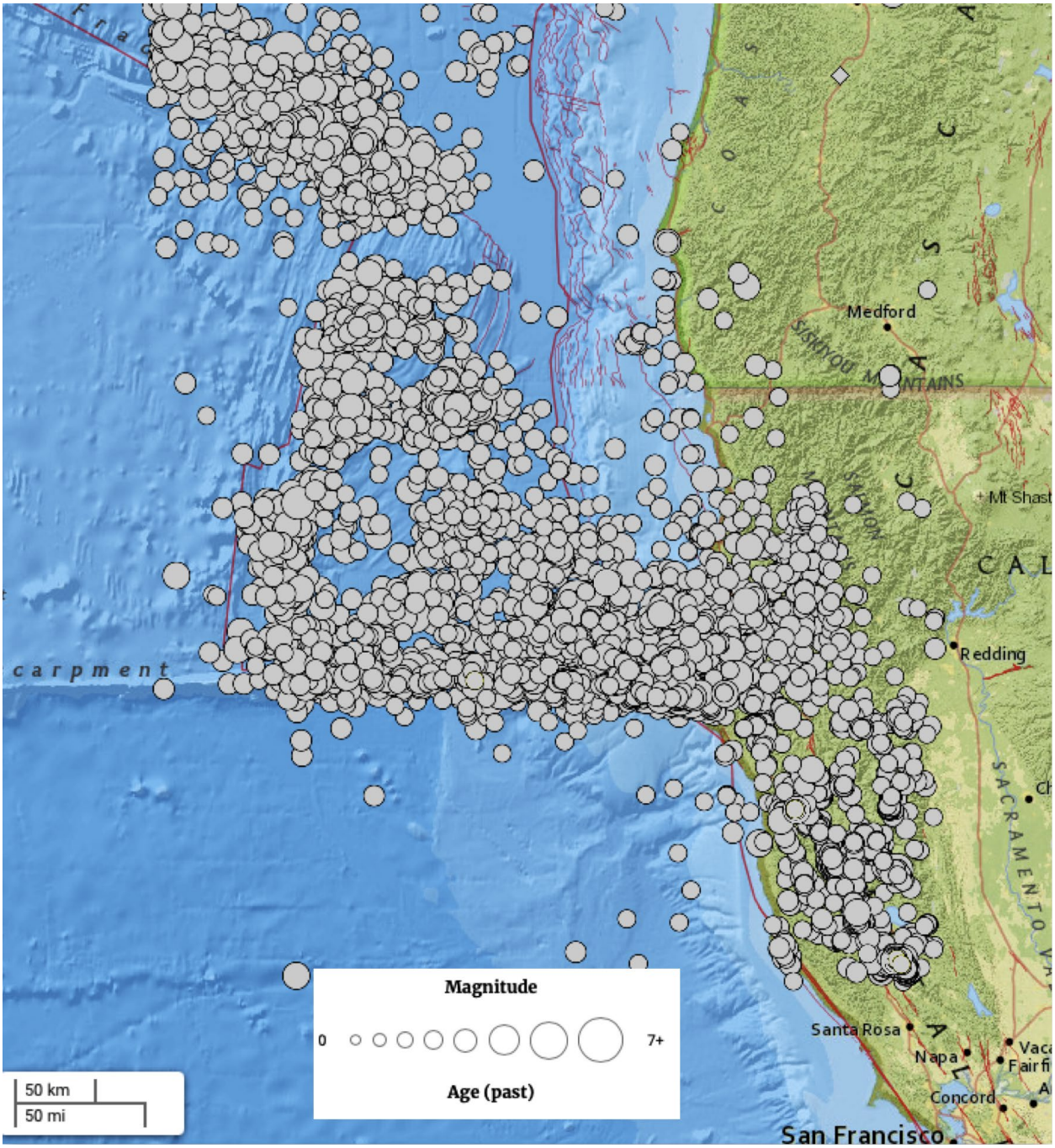

Figure 13. Map showing earthquakes > M2.5 in the North Coast region in the time period 2000-2024. Earthquakes south of Cape Mendocino (concealed by epicenters) are associated with the northwest striking San Andreas fault zone, Abrupt E-W trending seismicity offshore of Cape Mendocino are associated with the Mendocino fault. The majority of earthquakes, located north of Cape Mendocino are associated with deformation of the Gorda plate. There are little to no earthquakes associated with the locked Cascadia subduction zone or faults within the fold and thrust belt.

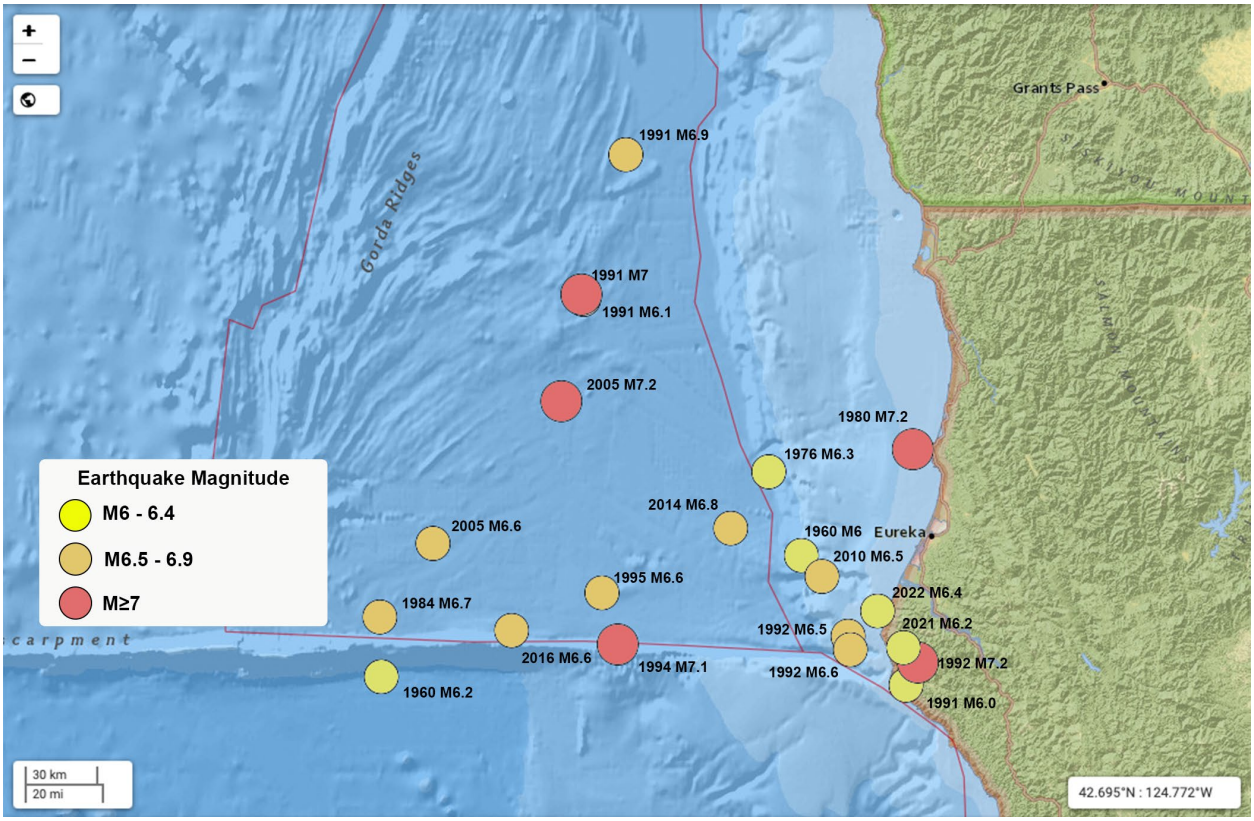

Figure 14. Regional earthquakes > M6 since 1960.

Table 5. Regional earthquakes > M6 since 1960 (between latitudes 40°-42 N and longitudes 127°-123°W.

Year	Magnitude (M)	Depth (km)	Epicenter location (decimal latitude, longitude)	Description	Event date/time	Data Source (USGS Earthquake Catalog)
1980	7.2	19.0	41.117°N 124.253°W	Gorda Plate; 5 miles NW of Trinidad. Large, left-lateral strike slip fault, striking N50E from the Mendocino Fracture Zone	1980-11-08 10:27:34 (UTC)	https://earthquake.usgs.gov/earthquakes/eventpage/usp0001aq1/executive
1991	7.0	1.3	41.679°N 125.856°W	Central Gorda Plate. Left-lateral strike-slip fault.	1991-08-17 22:17:09 (UTC)	https://earthquake.usgs.gov/earthquakes/eventpage/nc228064/executive
1992	7.2	9.9	40.335°N 124.229°W	Cape Mendocino (Petrolia). Oblique-slip fault with reverse component. Coseismic uplift of 1.5 m recorded at the coast near Petrolia. Generated tsunami with maximum wave heights (peak-to-trough) of 1.1 m at Crescent City. California, and 0.1 meters on	1992-04-25 18:06:05 (UTC) (11:06 am PDT)	https://earthquake.usgs.gov/earthquakes/eventpage/nc269151/executive

Year	Magnitude (M)	Depth (km)	Epicenter location (decimal latitude, longitude)	Description	Event date/time	Data Source (USGS Earthquake Catalog)
				Hawaii. Two large earthquakes (M6.5 and M6.6) occurred in the same area on the following day, 26 April 1992.		
1994	7.0	5.0	40.406°N 126.303°W	Mendocino Fracture Zone, 70 miles west of Cape Mendocino. Strike-slip fault	1994-09-01 15:15:48 (UTC)	https://earthquake.usgs.gov/earthquakes/eventpage/nc30056327/executive
2005	7.2	16.0	41.292°N 125.953°W	Central Gorda Plate, 110 km west of epicenter of 1980 M7.2 event. Northeast striking left-lateral strike-slip fault	2005-06-15 02:50:54 (UTC)	https://earthquake.usgs.gov/earthquakes/eventpage/usp000dt25/executive
1960	6.0	15.0	40.729°N 124.792°W	Gorda plate, 25 mile NW of Eel River	1960-06-06 01:17:53 (UTC)	https://earthquake.usgs.gov/earthquakes/eventpage/iscgem879414/executive
1976	6.3	41.8	41.035°N 124.950°W	Gorda plate, 35 mi NW of Eureka. Strike-slip fault	1976-11-26 11:19:32 (UTC)	https://earthquake.usgs.gov/earthquakes/eventpage/nc1032447/executive
1984	6.6	4.3	40.504°N 125.130°W	Gorda plate, 40 miles NW of Cape Mendocino	1984-09-10 03:14:28 (UTC)	https://earthquake.usgs.gov/earthquakes/eventpage/nc27615/executive
1991	6.1	2.5	41.661°N 125.846°W	Central Gorda Plate. Strike-slip fault with small reverse component.	1991-08-16 22:26:14 (UTC)	https://earthquake.usgs.gov/earthquakes/eventpage/nc227958/executive
1991	6.0	8.3	40.252°N 124.286°W	Cape Mendocino. Reverse (thrust) fault; mechanism poorly constrained.	1991-08-17 19:29:40 (UTC)	https://earthquake.usgs.gov/earthquakes/eventpage/nc228027/executive
1992	6.5	18.8 km	40.433°N 124.566°W	Cape Mendocino (Petrolia) / Gorda plate. This earthquake occurred less than 24 hours later and in the same area as the M7.2 earthquake on 25 April 1992. Strike-slip fault with small reverse component.	1992-04-26 07:41:40 (UTC) (12:42 am PDT)	https://earthquake.usgs.gov/earthquakes/eventpage/nc268031/executive
1992	6.6	21.7	40.383°N 124.555°W	Cape Mendocino (Petrolia) / Gorda Plate. Occurred less than 4 hours after the M6.5 earthquake, and less than 24 hours after the M7.2	1992-04-26 11:18:25 (UTC) (4:19 am PDT)	https://earthquake.usgs.gov/earthquakes/eventpage/nc268078/executive

Year	Magnitude (M)	Depth (km)	Epicenter location (decimal latitude, longitude)	Description	Event date/time	Data Source (USGS Earthquake Catalog)
				earthquake. Strike-slip fault with small reverse component.		
1995	6.6	4.6	40.592°N 125.757°W	Southern Gorda plate. Strike-slip fault.	1995-02-19 04:03:14 (UTC)	https://earthquake.usgs.gov/earthquakes/eventpage/nc30068187/executive
2010	6.5	28.7	40.652°N 124.693°W	Southern Gorda Plate, 20 miles W of Eel River. Near vertical strike-slip fault striking N47E.	2010-01-10 00:27:39 (UTC)	https://earthquake.usgs.gov/earthquakes/eventpage/nc71338066/executive
2014	6.8	16.4	40.829°N 125.134°W	Southern Gorda Plate, 40 miles W of Eureka. Oblique-slip fault with reverse component.	2014-03-10 05:18:13 (UTC)	https://earthquake.usgs.gov/earthquakes/eventpage/nc72182046/executive
2016	6.6	8.5	40.454°N 126.194°W	Mendocino Fracture Zone. Right-lateral strike-slip fault.	2016-12-08 14:49:45 (UTC)	https://earthquake.usgs.gov/earthquakes/eventpage/us20007z6r/executive
2021	6.2	27	40.390°N 124.298W	Southern Gorda plate near Petrolia	2021-12-20 20:10:31(UTC)	https://earthquake.usgs.gov/earthquakes/eventpage/nc73666231/executive
2022	6.4	17.9	40.525°N 124.423W	Gorda plate, 9 miles WSW of Ferndale, CA	2022-12-20 10:34:24(UTC)	https://earthquake.usgs.gov/earthquakes/eventpage/nc73821036/executive

The most recent earthquakes of greatest concern in terms of the built environment on the North Coast were the 1980 M7.2 earthquake; the 1992 M7.2 earthquake and associated M6.5 and M6.6 aftershocks; the 2010 M6.5 earthquake and the 2021 M6.2 and 2022 M6.4 earthquakes. Several other sizeable earthquakes during that time period include two earthquakes in the Gorda plate in 1991 (M7.0) and 2005 (M7.2), and an M7.2 earthquake on the Mendocino fault in 2005, but each of these were too distant (>130 km) to generate strong shaking onshore[2] (Figure 17) (Dengler et al., 1995; USGS, 2020i). There was also a strong earthquake in 1954 that caused damage, including from liquefaction, in the Eureka-Arcata area. The size of this earthquake is estimated as M6.5 (USGS, 2020b), but it is not well

[2] USGS MMI shake maps show low intensity levels for 3 earthquakes >M7.0 in the Gorda plate and Mendocino fault that, although large, were also distant from shore: (1) 1991 M7.0 <https://earthquake.usgs.gov/earthquakes/eventpage/nc228064/map>; (2) 2005 M7.2 https://earthquake.usgs.gov/earthquakes/eventpage/usp000dt25/map ; and (3) 1994 M7.2 https://earthquake.usgs.gov/earthquakes/eventpage/nc30056327/map.

documented as it occurred prior to the launch of the NCSS network. Bakun (2000, p. 799) used historical records of shaking intensity in Northern California and coincident reports in more distant areas in California and Oregon to propose that earthquakes > M7.0 may have also occurred either in the Gorda plate or Mendocino fault in 1873, 1878, 1899, 1923, and 1945.

3.1 1980 M7.2 Earthquake

The M7.2 earthquake on November 8, 1980 was the largest event for the North Coast region in several decades (USGS, 2020f). According to eyewitness accounts, strong shaking lasted locally for 15-20 seconds, and shaking was felt as far away as San Francisco and Salem, Oregon (Lajoie and Keefer, 1981). The epicenter was relatively deep in the Gorda plate (19 km) along a northeast-southwest trending left-lateral strike slip fault (Kilbourne and Saucedo, 1981; Rollins and Stein, 2010; USGS, 2020f) (Figures 7, 17). Previous analyses have described the distance of the epicenter from shore as about 50-60 km (30-37 mi) west-northwest of Trinidad, California (Lajoie and Keefer, 1981; Rollins and Stein, 2010) (Figure 7). More recent data from the USGS (USGS, 2020f) shows the epicenter much closer to shore at 8 km (5 miles) (Figures 14, 15).

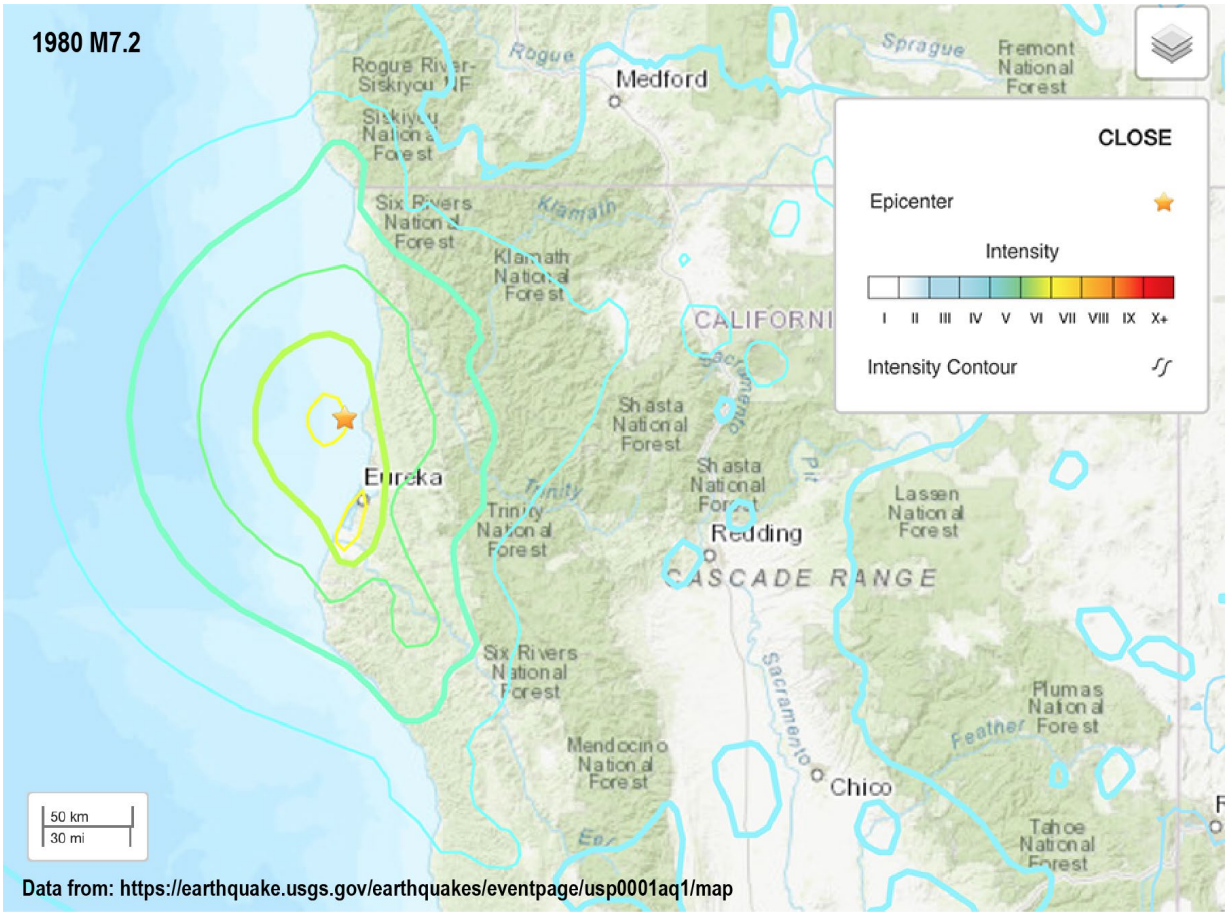

Figure 15. USGS MMI shake map for the 1980 M7.2 earthquake.

Shaking intensity reached levels VI-VII in the greater Humboldt Bay area (Figure 15). Although structural damage in the area was not extensive, the effects from shaking caused liquefaction and ground failure (slumps and slides) in both onshore and offshore environments of the North Coast (Field et al., 1981; Lajoie and Keefer, 1981; Field, 1984, 1993).

Lajoie and Keefer (1981) completed a post-earthquake reconnaissance study in which they looked for evidence of damage from both the ground and from overhead flights of the area. They reported (p. 4) that structural damage in the area was minimal with severe damage limited to few homes and buildings that were poorly constructed and failed easily in Fields Landing or on the North Spit/Samoa Peninsula. In the areas of strongest shaking, most damage associated with buildings consisted of broken windows, collapsed chimneys, and damage to objects displaced from shelves. For example, no structural damage was reported at any of the numerous buildings at the lumber mill sites on the North Spit/Samoa Peninsula (p. 8). The PG&E power plant at Buhne Point was briefly shut down as a precautionary measure, but neither the main power plant nor cold-storage nuclear facility sustained any damage (p. 9). Failure of a highway overpass on Highway 101 at Thompkins Hill Road, which resulted in 2 vehicle crashes and 6 injuries, was attributed to poor design that allowed the supports for the overpass to be dislodged from their footings as a result of the shaking (Lajoie and Keefer, 1981; Imbsen, 1981). The overpass was scheduled for a reinforcement upgrade by Caltrans in 1981, as it had already been determined that it had previously sustained minor damage by an earthquake in 1975 (Lajoie and Keefer, 1981, p. 16).

The shaking triggered numerous small slumps and landslides in the area, and the effects of liquefaction, primarily in the area of intensity level VII, were evident from cracks in roads and parking lots built over presumably water-saturated alluvial deposits (Kilbourne and Saucedo, 1981; USGS, 2020f). Kilbourne and Saucedo (1981, p. 55) noted that, based on comparison of the 1980 earthquake with previous events, surface ground failures in areas of high intensity shaking are “very repetitive in occurrence” in the Humboldt region.

Offshore, the 1980 M7.2 earthquake triggered a large submarine landslide in about 60 m of water on the continental shelf south of the Klamath River (Field et al., 1981, 1982; Field, 1984, 1993; Field and Jennings, 1987). The slide was the result of liquefaction and degassing of the seafloor sediment, displacing an area of about 20 km^2 on a nearly flat surface.

3.2 1992 M7.2 Earthquake

The 1992 “Cape Mendocino earthquakes” consisted of a M7.2 mainshock on April 25 followed by a series of aftershocks, the largest of which were M6.5 and M6.6 earthquakes on April 26 (Reagor and Brewer, 1992; Velasco et al., 1994; Toppozada and Branum, 2004). The M7.2 mainshock occurred onshore at Cape Mendocino at a depth of 9.9 km and about 4 km (2.5 mi) west of the town of Petrolia (Murray et al., 1996; Oppenheimer et al., 1993; Reagor & Brewer, 1992, USGS, 2020d) (Figures 14 and 16). The M6.5 and M6.6 aftershocks occurred on strike-slip faults in the Gorda plate about 30 km (19 mi)

offshore of Cape Mendocino and at depths of 18.8 km and 21.7 km, respectively, (USGS, 2020c, 2020e) (Figures 17, 18).

Combined impacts from the earthquakes on April 25-26 resulted in more than 350 injuries and approximately $75 million in damage to homes, businesses, roads, and bridges, mainly in the communities between the Eel River valley and Scotia (O'Brien, 1992; Toppozada and Branum, 2004). Shaking intensities for the M7.2 event reached level IX in the Cape Mendocino area and VI-VIII in areas encompassing Humboldt Bay (Figure 16). The aftershocks also produced level VIII intensities in the vicinity of Cape Mendocino and V-VII in the Humboldt Bay area (Figures 17, 18). Compared to communities south of Humboldt Bay, damage in Eureka and Arcata was minimal (O'Brien, 1992; Toppozada and Branum, 2004).

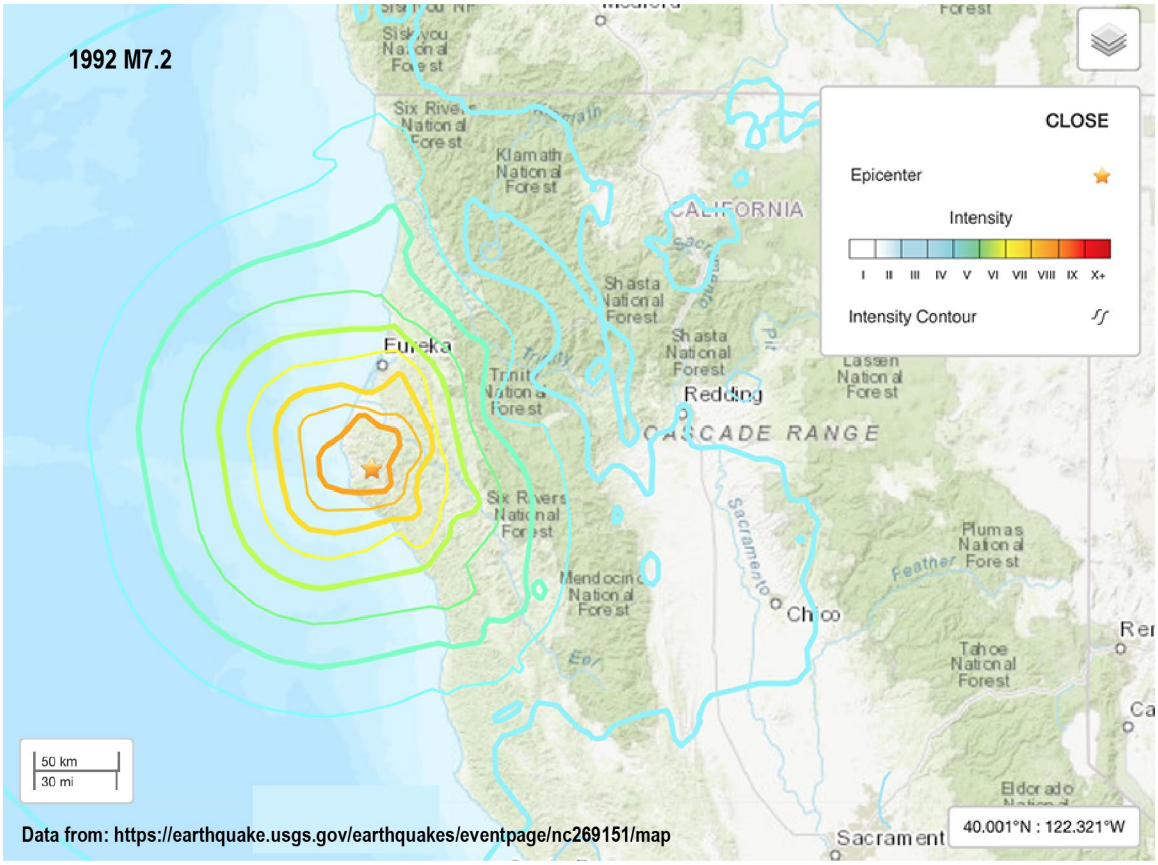

Figure 16. USGS MMI shake map for the 1992 M7.2 Cape Mendocino earthquake.

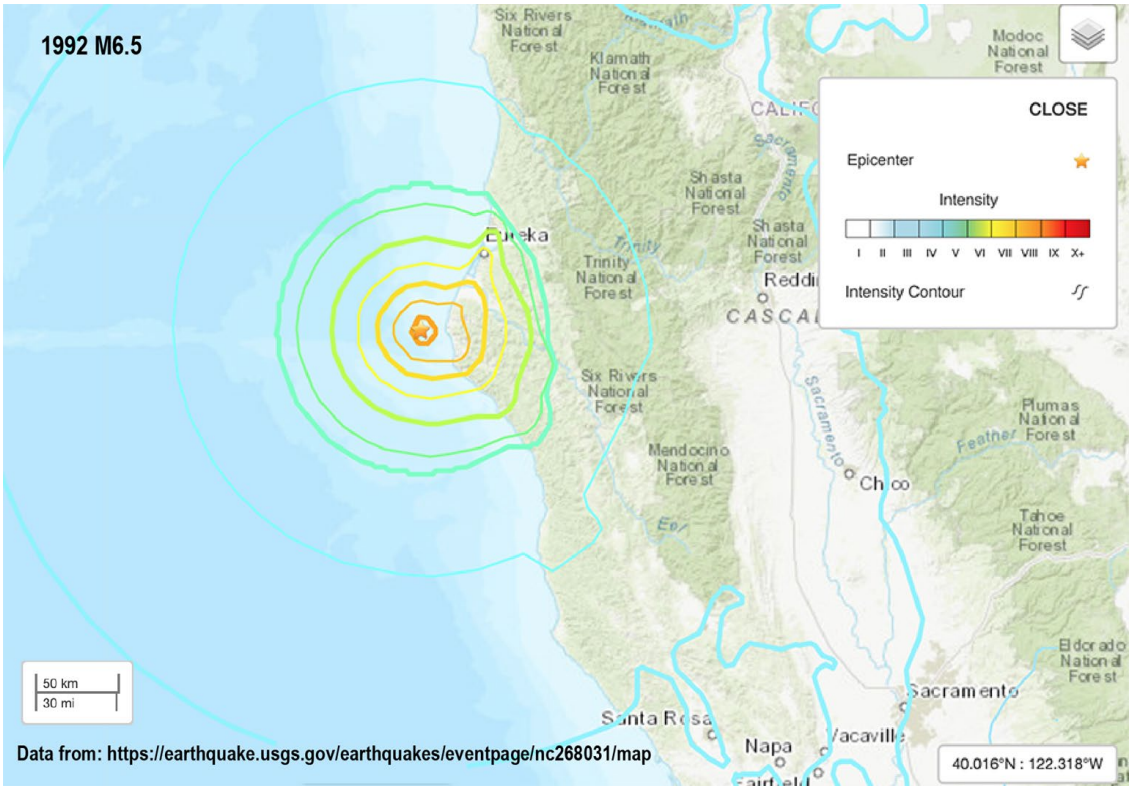

Figure 17. USGS MMI shake map for the April 26, 1992 M6.5 Cape Mendocino earthquake aftershock.

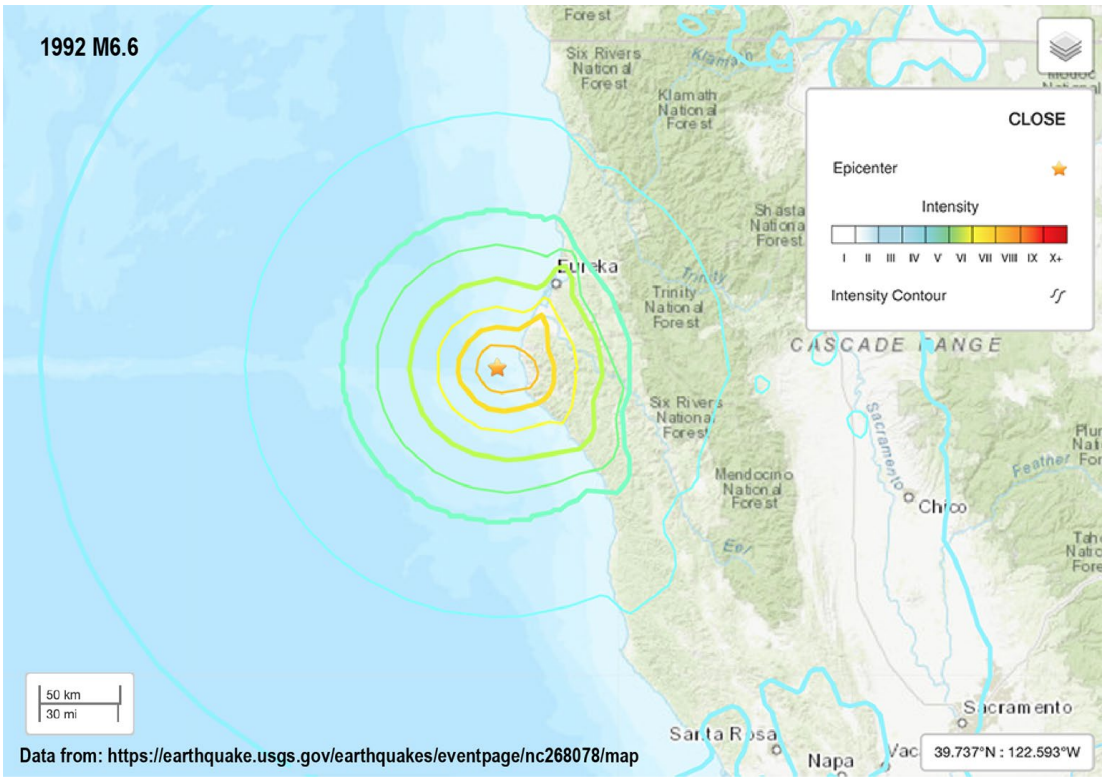

Figure 18. USGS MMI shake map for the April 26, 1992 M6.6 Cape Mendocino earthquake aftershock.

Fault offset during the M7.2 event resulted in 1.4 m of permanent uplift along a 15 km long stretch of the coast from Cape Mendocino to south of Punta Gorda (Green and Sawyer, 1993; Merritts, 1996), and generated a small, non-destructive tsunami that reached Eureka followed by Crescent City in less than 1 hour (González et al., 1995). Landslides, mostly older features that were reactivated by the shaking, were widespread in the areas of greatest impact (Reagor and Brewer, 1992; Green and Sawyer, 1993). Liquefaction features, including sand boils 20 m across, were observed in saturated alluvial deposits in the Eel and Mattole rivers valleys (Reagor and Brewer, 1992; Green and Sawyer, 1993).

A prevailing theory is that the M7.2 mainshock represented rupture along the Cascadia megathrust (Green and Sawyer, 1993; Oppenheimer et al., 1993). However, more recent research strongly supports rupture along a parallel thrust fault above the megathrust in the upper plate/accretionary wedge (Vermeer and Hemphill-Haley, 2014; Vermeer et al., 2015; Vermeer, 2016; Hartshorn et al., 2017; Crawford, 2019). Regardless, the mainshock and associated aftershocks are further examples of the geologically frequent deformation occurring in the tectonically active MTJ region (Merritts, 1996).

3.3 2010 M6.5 Earthquake

The M6.5 earthquake on January 9, 2010, was located on a northeast-striking left lateral strike-slip fault in the Gorda plate about 48km (30 mi) west-northwest of Eureka and at a depth of 28.7 km (Bonowitz et al., 2010; Storesund et al., 2010; Berkeley Seismological Laboratory, 2020; USGS, 2020d) (Figure 19, Table 5). It was the largest earthquake in the region since two M7.2 events in 1992 and 2005. Although the magnitude of the 2010 event was significantly smaller than the M7.2 earthquakes in 1992 and 2005, the closer proximity of the 2010 earthquake epicenter and fault orientation relative to Eureka and Humboldt Bay resulted in more widespread damage compared to those earlier events (Storesund et al., 2010).

Shaking from the earthquake was strongest near the coast between Petrolia and Eureka (Figure 19), with MMI levels of VI-VIII (USGS, 2020d) (Figure 22). Shaking was most severe in Eureka (Storesund et al., 2010), reaching 33% g in Eureka and 44% g in Ferndale (Bonowitz et al., 2010). Damage to buildings and homes in Eureka and Ferndale was moderate to severe, and 30 people were injured (Bonowitz et al., 2010).

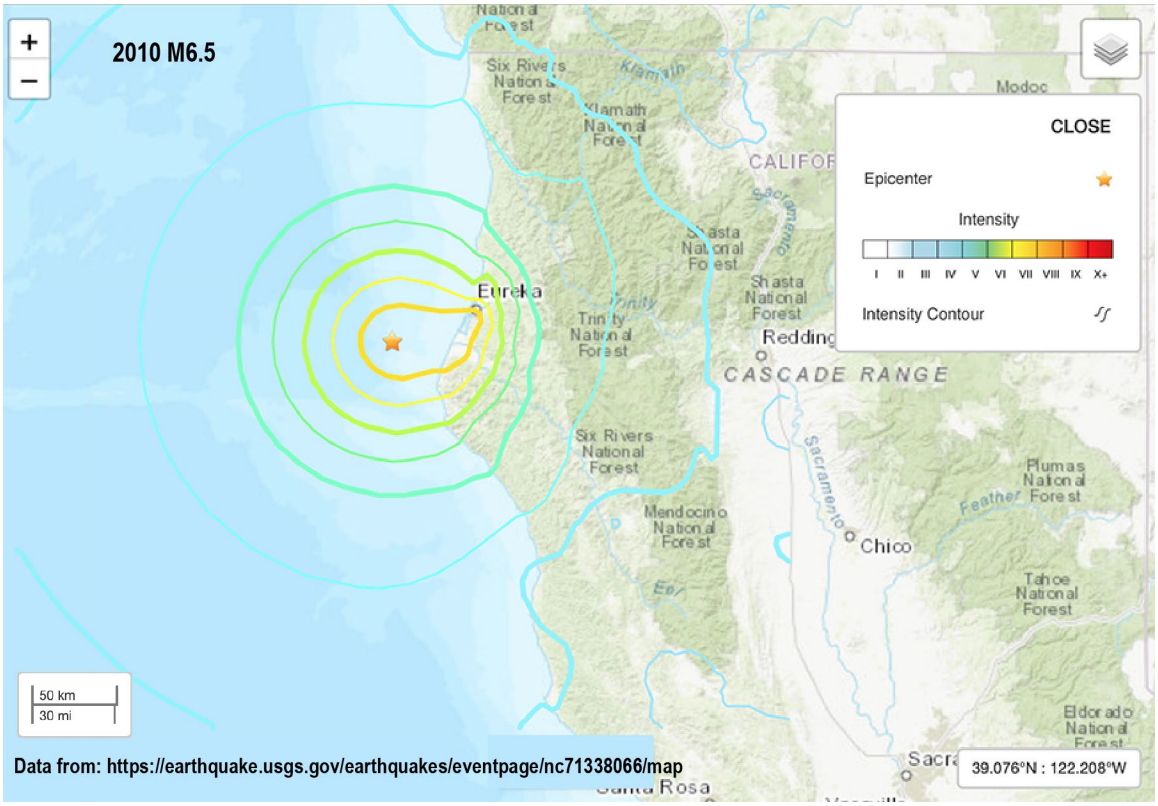

Figure 19. USGS MMI shake map for the 2010 M6.5 earthquake.

Storesund et al. (2010) and Bonowitz et al. (2010) provided a detailed account of the effects of the M6.5 event in their post-earthquake reconnaissance reports. They reported that about 800 homes and buildings sustained damage, 10 of which included major damage. Estimated losses at the time of the report totaled $40 million, but they also noted (p. 1) that buildings in Eureka that had been retrofitted in keeping with the city's 1989 Unreinforced Masonry (URM) sustained little more than "cosmetic damage." Landslides were frequent along steep slopes at the coast, which Storesund et al. (2010, p. 10) noted was an expected occurrence because of the characteristic unstable slopes in this area and the proximity of the earthquake epicenter. Their observations supported Keefer's (1984) empirical model for the earthquake-generated landslides, with M6.5 earthquakes capable of triggering landslides in appropriate terrain within a 150 km radius of the earthquake epicenter. Liquefaction features (sand boils and lateral spreading) were present in saturated sediment at Centerville Beach and along the Eel River (Bonowitz et al., 2010; Storesund et al., 2010, p. 15), and several asphalt parking lots in Eureka showed minor cracks attributed to liquefaction of underlying alluvial sediment (Storesund et al., 2010, p. 19). Although widely distributed, no serious damage from liquefaction, lateral spreading, or ground settling was reported in the greater Humboldt Bay area from this event.

3.4 2021 M6.2 Earthquake

The December 20, 2021 M6.2 earthquake occurred in the southern Gorda plate and eastern Mendocino fault area (Figures 20, 21). The earthquake was preceded by 11 seconds by a M5.7 earthquake possibly along the Mendocino fault 30 km to the west of the mainshock (US Geological Survey, 2021). The M6.2 event occurred near Petrolia and was likely within the Gorda plate (US Geological Survey, 2021). These earthquakes occurred in the general area of the 1992 M6.5, 6.6 and 7.2 earthquake sequence described earlier in this report. Yoon and Shelly (2024) and Shelly et al. (2024) report that the foreshock was a M6.1 and not M5.7 event. Yeck et al. (2023) evaluated these two events, separated by 11 seconds and 30 km, and concluded that the complexity of structures at this part of the Cascadia subduction allowed two distinct faults separated by a significant distance to interact and cause dynamic rupture. This kind of behavior, observed on larger faults with correspondingly large magnitude earthquakes (e.g., 2016 M7.9 Kaiköura, NZ (Litchfield et al., 2017) has profound implications on our ability to assess seismic hazards on faults capable of producing moderate earthquakes that may interact with nearby or even distant faults.

Shaking from the M6.2 event was strongly felt throughout northern California. MMI VIII was described in the vicinity of Cape Mendocino while the project area and Eureka, immediately to the south, experienced MMI III to IV ground shaking (Figure 20).

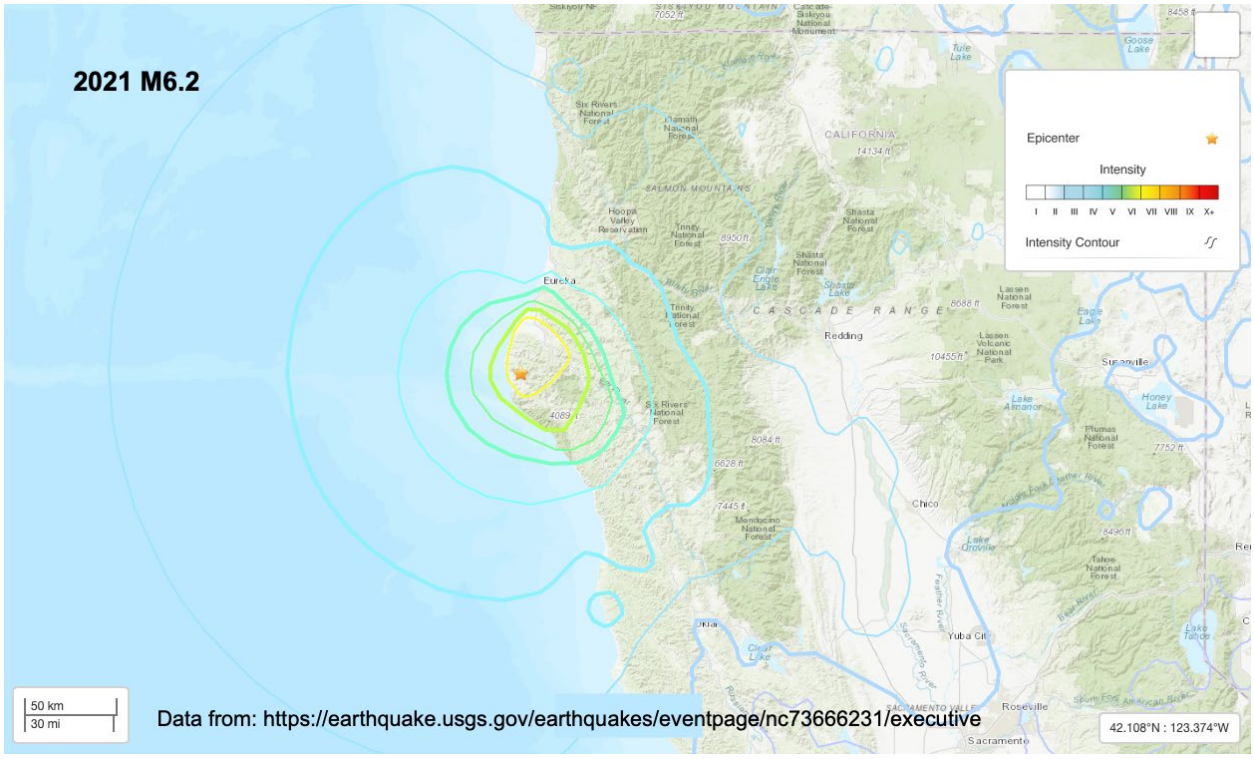

Figure SEQ Figure * ARABIC 20. USGS MMI shake map for the 2021 M6.2 earthquake.

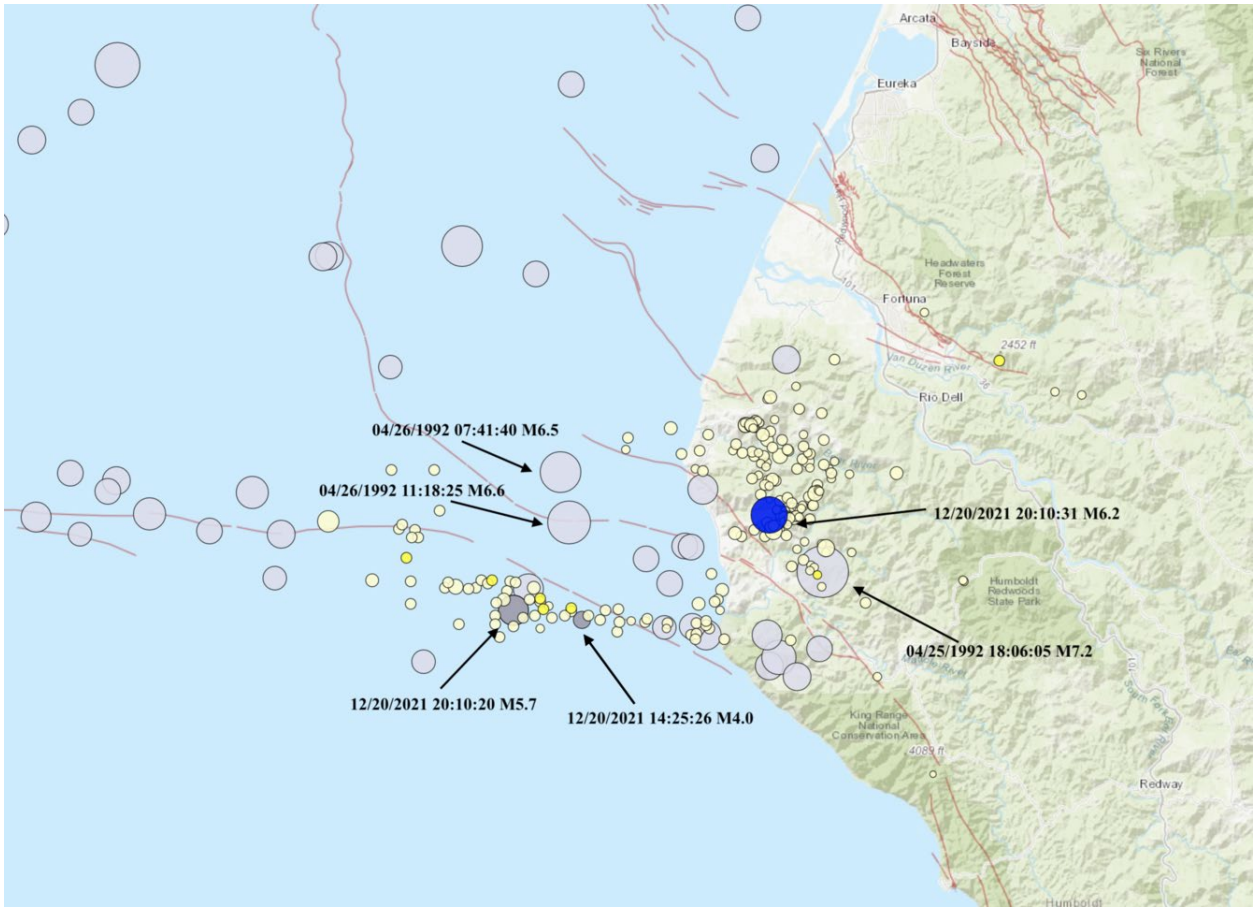

Figure SEQ Figure * ARABIC 21. Epicentral map for the 2021 M5.7 and 6.2 earthquakes with respect to locations of the 1992 M 6.5, 6.6 and 7.2 earthquakes. Source https://www.usgs.gov/media/images/map-showing-revised-location-m62-petrolia-earthquake-12202021.

3.5 2022 M6.4 earthquake

The December 20, 2022 M6.4 earthquake occurred immediately offshore of Cape Mendocino about 15 km (9.3 mi) southwest of Ferndale (Figure 22). This event occurred about 20 km to the northeast of the 2021 M6.2 earthquake (US Geological Survey, 2022). The earthquake produced significant ground motions, in places reported as much as 30 – 140% g (Stein et al., 2023). The east-northeast oriented rupture may have contributed to directed ground motions toward the north.

Yoon and Shelly (2024) and Shelly et al. (2024) evaluated the 2022 earthquake as well as the 2021 M6.1 and 6.2 events. They concluded that the three events all occurred within the Gorda plate but at different depths within the oceanic slab. They also conclude that some afterslip may have occurred on the megathrust as a result of these events.

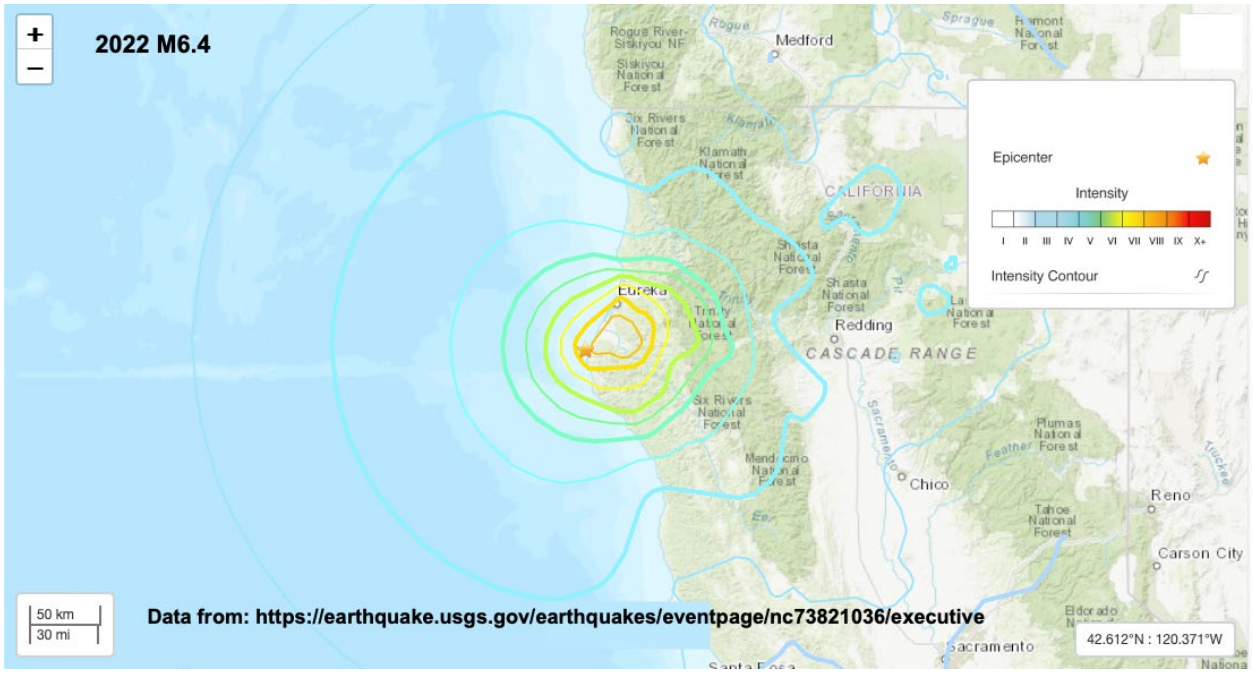

Figure SEQ Figure * ARABIC 22. USGS MMI shake map for the 2022 M6.4 earthquake.

4 Strong Motion along HWY 101 Safety Corridor

Seismic events are typically associated with strong motion. The intensity of shaking is a function of the size and location of the earthquake from a particular site, the site conditions (i.e., geologic materials, level of saturation, topography), the travel path of seismic waves and the attenuation properties of the materials the waves traverse.

Previous evaluations of potential strong motion of the project area have been described (CalTrans Geotechnical Services, 2006). A Peak Bedrock Acceleration estimate was reported at 0.7g based on a M6.75 earthquake on the Fickle Hill fault. Additionally, PG&E has developed strong motion probabilistic and deterministic curves specific to the Humboldt Bay Power Plant and Independent Spent Fuel Storage Installation (ISFSI) (Pacific Gas and Electric Company, 2017) that consider regional events including the sources listed here. Although these are not specific to the project that may be considered for a detailed analysis.

As a cursory analysis of the conditions along the Hwy 101 project the American Society of Civil Engineering has developed an online tool for evaluating ground motions considering levels of risk and site conditions (https://ascehazardtool.org). The general area of western Humboldt County, and specifically Humboldt Bay is categorized as having Peak Ground Acceleration (PGA) of 2% in 50 yrs, from the National Seismic Hazard Map of between 2.4 and 3.4% (Figure 23).

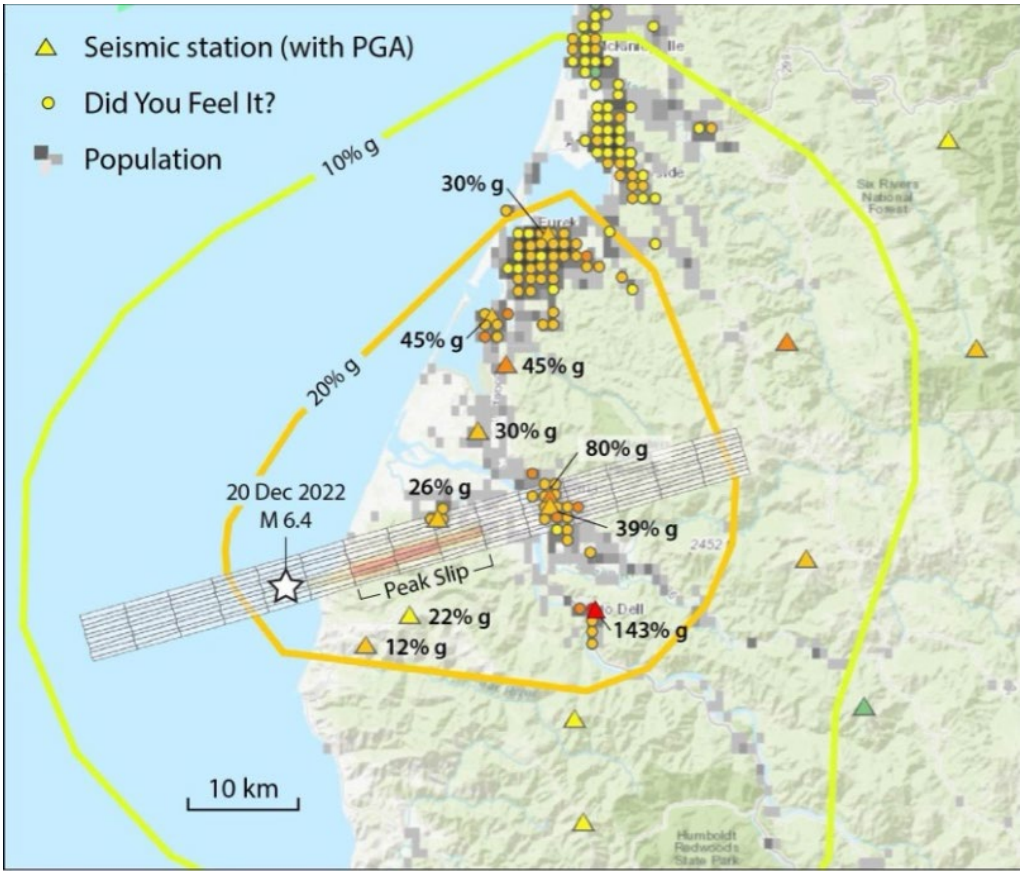

Figure SEQ Figure * ARABIC 23. Seismic shaking in terms of %g as a result of the 2022 M6.4 earthquake (white start represents the epicenter). Gridded bar represents slip amounts at depth along a ENE striking fault. Contours are in 10% g increments. Colored triangles represent PGA measured at seismic stations. Circles are interpreted ground motions from public felt reports. Significant ground shaking was recorded in the vicinity of the project area (from Stein et al., 2023).

Using the ASCE hazard tool, specifically along the HWY 101 corridor, and considering a range of conditions from hard rock, dense and soft rock, and stiff clay, the estimated PGA of 2% in 50 yrs ranges from 1.1 to 1.6 g, respectively (Figures 24-27).

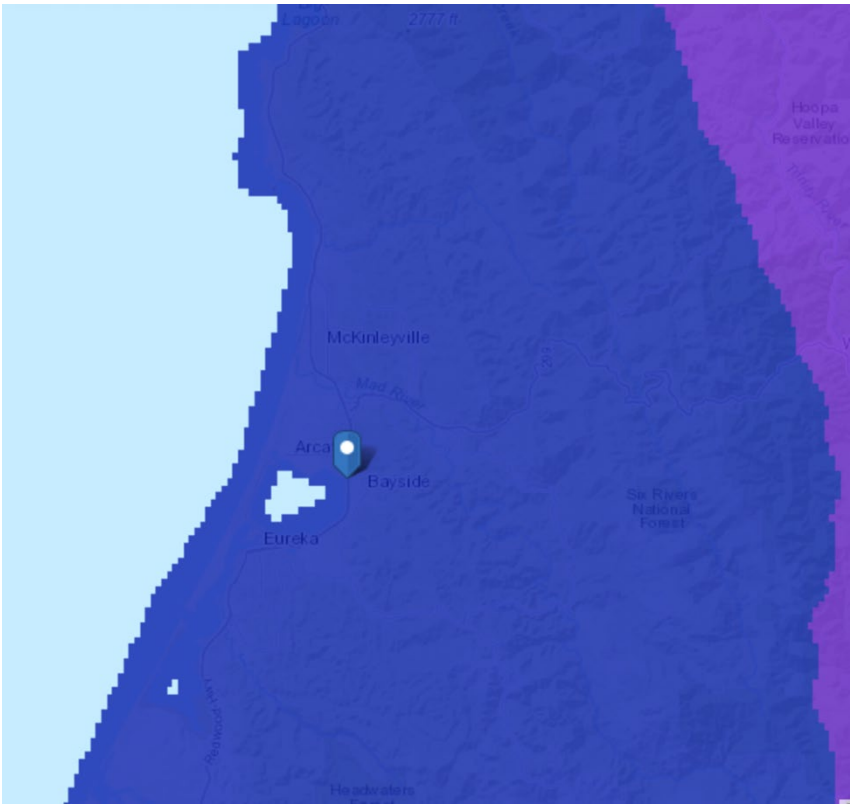

Figure SEQ Figure * ARABIC 24. Potential ground motions (PGA, 2% in 50 yrs) from the National Seismic Hazard Map (from https://ascehazardtool.org). The generalized map of the area surrounding the Humboldt Bay area is projected to be within 2.37-3.45g).

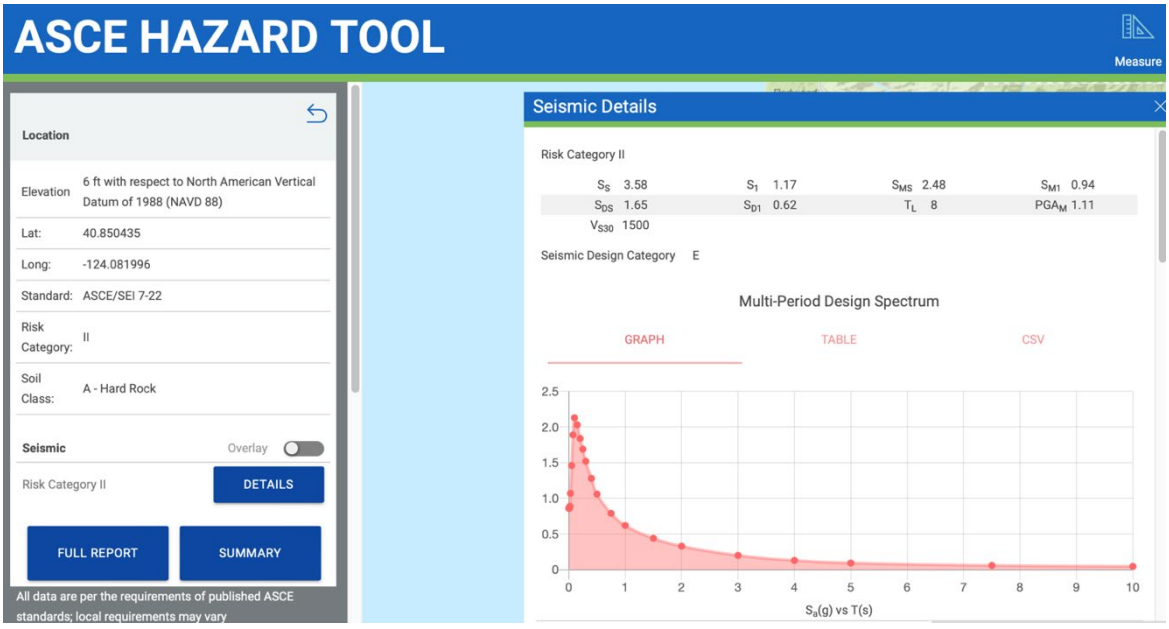

Figure 25. An evaluation of a location along Highway 101 (site location is on Figure 23) for hard rock conditions results in a PGA of 1.11 g.

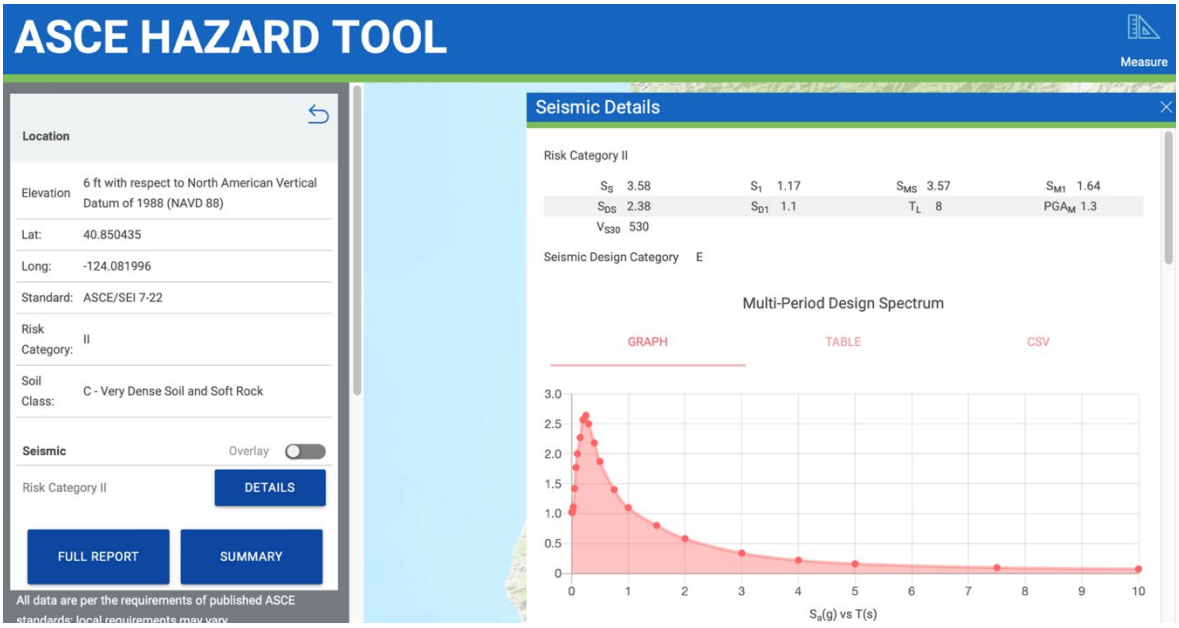

Figure 26. An evaluation of location along Highway 101 (site location is on Figure 23) for dense and soft rock conditions results in a PGA of 1.3 g.

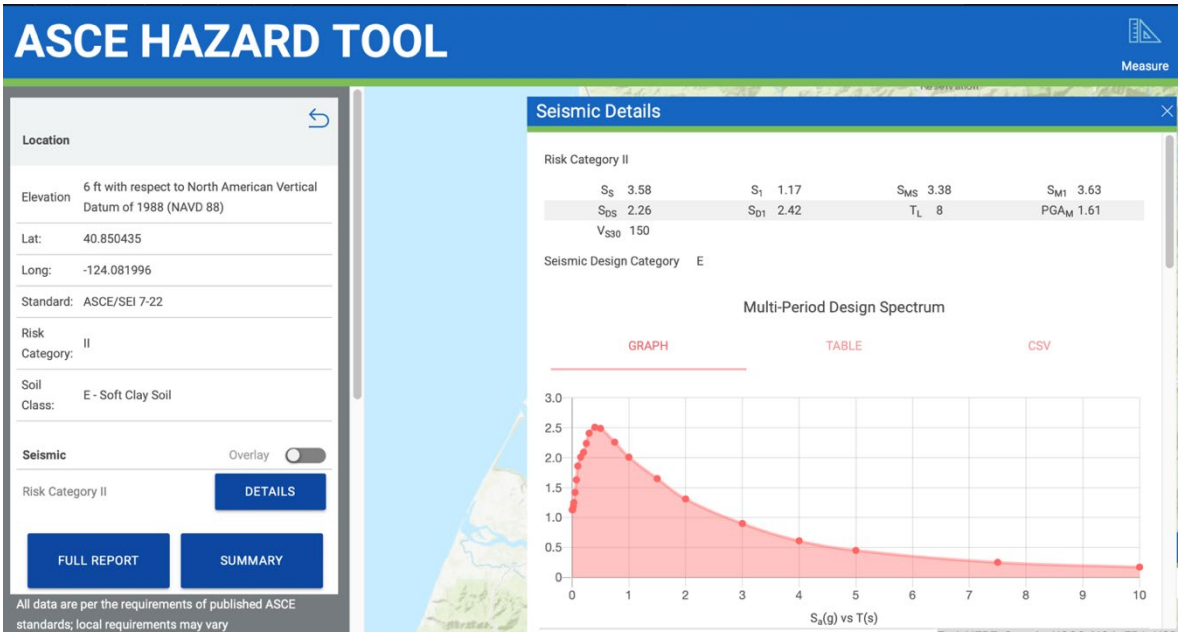

Figure 27. An evaluation of location along Highway 101 (site location is on Figure 23) for soft clay soil conditions results in a PGA of 1.61 g.

5 REFERENCES

Abramson, H.F., 1998, Evidence for tsunamis and earthquakes during the last 3500 years from Lagoon Creek, a coastal freshwater marsh, northern California [Masters Thesis]: Humboldt State University, 87 p.

Atwater, B.F., 1987, Evidence for Great Holocene Earthquakes Along the Outer Coast of Washington State: Science, v. 236, p. 942–944, doi:10.1126/science.236.4804.942.

Atwater, T., 1989, Plate tectonic history of the northeast Pacific and western North America, *in* Winterer, E.L., Hussong, D.M., and Decker, R.W. eds., The Eastern Pacific Ocean and Hawaii, North America, Geological Society of America, p. 21–72, doi:10.1130/DNAG-GNA-N.21.

Atwater, B.F., Musumi-Rokkaku, S., Satake, K., Tsuji, Y., Ueda, K., and Yamaguchi, D.K., 2005, The orphan tsunami of 1700—Japanese clues to a parent earthquake in North America: Seattle, WA / Washington, D.C., University of Washington Press and U.S. Geological Survey Professional Paper 1707, 135 p., http://pubs.er.usgs.gov/publication/pp1707 (accessed May 2020).

Bakun, W.H., 2000, Seismicity of California's North Coast: Bulletin of the Seismological Society of America, v. 90, p. 797–812, doi:10.1785/0119990138.

Bakun, W.H., and Prescott, W.H., 1993, The Loma Prieta, California, Earthquake of October 17, 1989: Earthquake occurrence: U.S. Geological Survey USGS Professional Paper 1550, http://pubs.er.usgs.gov/publication/pp1550 (accessed April 2020).

Beeson, J.W., Johnson, S.Y., and Goldfinger, C., 2017, The transtensional offshore portion of the northern San Andreas fault: Fault zone geometry, late Pleistocene to Holocene sediment deposition, shallow deformation patterns, and asymmetric basin growth: Geosphere, p. GES01367.1, doi:10.1130/GES01367.1.

Berkeley Seismological Lab, 2020, When Creep becomes Unsteady: Seismo Blog, https://seismo.berkeley.edu/blog/2018/06/19/when-creep-becomes-unsteady.html (accessed April 2020).

Berkeley Seismological Laboratory, 2020, M6.5 Gorda plate earthquake offshore of Northern California, 16:27 PST January 9, 2010: Berkeley Seismologial Lab: Information from the CISN Northern California Management Center, USGS & UC Berkeley, https://www.cisn.org/special/evt.10.01.10/ (accessed May 2020).

Boatwright, J., and Bundock, H., 2005, Modified Mercalli Intensity Maps for the 1906 San Francisco Earthquake Plotted in ShakeMap Format: U.S. Geological Survey Open-File Report 2005–1135, https://pubs.usgs.gov/of/2005/1135/ (accessed April 2020).

Bonowitz, D., Dengler, L.A., and Lizundia, Bret, 2010, The Mw6.5 offshore northern California earthquake of January 9, 2010: Earthquake Engineering Research Institute EERI Special Earthquake Report, 12 p., https://eeri.org/site/images/eeri_newsletter/2010_pdf/January_9_OffshoreNorCal.pdf.

Bryant, W.A., 2001, Fault number 18, Mendocino fault zone: Quaternary fault and fold database of the United States: U.S. Geological Survey website, https://earthquake.usgs.gov/cfusion/qfault/show_report_AB_archive.cfm?fault_id=18&section_id= (accessed January 2020).

Burger, R.L., Fulthorpe, C.S., Austin, J.A., and Gulick, S.P.S., 2002a, Lower Pleistocene to present structural deformation and sequence stratigraphy of the continental shelf, offshore Eel River Basin, northern California: Marine Geology, v. 185, p. 249–281, doi:10.1016/S0025-3227(02)00196-2.

Burger, R.L., Fulthorpe, C.S., Austin, J.A., and Gulick, S.P.S., 2002b, Lower Pleistocene to present structural deformation and sequence stratigraphy of the continental shelf, offshore Eel River Basin, northern California: Marine Geology, v. 185, p. 249–281, doi:10.1016/S0025-3227(02)00196-2.

CalTrans Geotechnical Services, 2006, Preliminary structural geotechnical recommendations: Memorandum 01-Hum-101-KP130.09 PM 80.8, 6 p.

Carbotte, S.M. et al., 2024, Subducting plate structure and megathrust morphology from deep seismic imaging linked to earthquake rupture segmentation at Cascadia: Science Advances, v. 10, p. eadl3198, doi:10.1126/sciadv.adl3198.

Carver, G.A., 1992, Late Cenozoic Tectonics of Coastal Northern California, *in* Carver, G.A. and Aalto, K.R. eds., Field Guide to the Late Cenozoic Subduction Tectonics & Sedimentation of North Coastal California, Pacific Section of AAPG, p. 1–9, http://archives.datapages.com/data/pacific/data/087/087001/1_ps0870001.htm (accessed May 2020).

Carver, G.A., Abramson, H.A., Garrison-Laney, C.E., and Leroy, T., 1998, Investigation of paleotsunami evidence along the north coast of California: Unpublished report prepared for Pacific Gas and Electric Co, San Francisco, CA, v. 167, p. 238.

Carver, G.A., and Burke, R.M., 1988, Trenching investigations of northwestern California faults, Humboldt Bay Region, Final Report: US Geological Survey National Earthquake Hazards Reduction Program USGS NEHRP Final Report 14-08-0001-G1082, 51 p.

Chaytor, J.D., Goldfinger, C., Dziak, R.P., and Fox, C.G., 2004, Active deformation of the Gorda plate: Constraining deformation models with new geophysical data: Geology, v. 32, p. 353, doi:10.1130/G20178.2.

Choi, B.H., Hong, S.J., and Pelinovsky, E., 2006, Distribution of runup heights of the December 26, 2004 tsunami in the Indian Ocean: Geophysical Research Letters, v. 33, doi:10.1029/2006GL025867.

Cifuentes, I.L., 1989, The 1960 Chilean earthquakes: Journal of Geophysical Research: Solid Earth, v. 94, p. 665–680, doi:10.1029/JB094iB01p00665.

Clarke, S.H., and Carver, G.A., 1992, Late Holocene Tectonics and Paleoseismicity, Southern Cascadia Subduction Zone: Science, v. 255, p. 188–192, doi:10.1126/science.255.5041.188.

Crawford, B., 2019, Holocene marine terrace formation near the Mendocino triple junction: paleoseismic history derived from high resolution lidar, *in* GSA, https://gsa.confex.com/gsa/2019CD/webprogram/Paper329671.html (accessed June 2020).

Dengler, L.A., 2008, The 1906 Earthquake on California's North Coast: Bulletin of the Seismological Society of America, v. 98, p. 918–930, doi:10.1785/0120060406.

Dengler, L.A., Moley, K., McPherson, R., Pasyanos, M., Dewey, J.W., and Murray, M., 1995, The September 1, 1994 Mendocino fault earthquake: California Geology, v. 48, p. 43–53.

Dengler, L.A., Nicolini, T., Larkin, D., and Ozaki, V., 2008, Building Tsunami-Resilient Communities in Humboldt County, California: Solutions to Coastal Disasters 2008, p. 178–191, doi:10.1061/40978(313)17.

Didenkulova, I., Nikolkina, I., Pelinovsky, E., and Zahibo, N., 2010, Tsunami waves generated by submarine landslides of variable volume: analytical solutions for a basin of variable depth: Natural Hazards and Earth System Science, v. 10, p. 2407–2419, doi:10.5194/nhess-10-2407-2010.

Dziak, R.P., Fox, C.G., Bobbitt, A.M., and Goldfinger, C., 2001, Bathymetric Map of the Gorda Plate: Structural and Geomorphological Processes Inferred from Multibeam Surveys: Marine Geophysical Researches, v. 22, p. 235–250, doi:10.1023/A:1014606407111.

Earthweb, 2020, 1964 Prince William Sound Tsunami: Earthweb - University of Washington Earth and Space Sciences, https://earthweb.ess.washington.edu/tsunami/general/historic/alaska64.html (accessed May 2020).

Ellsworth, W.L., Lindh, A.G., Prescott, W.H., and Herd, D.G., 2013, The 1906 San Francisco Earthquake and the Seismic Cycle, *in* Earthquake Prediction, American Geophysical Union (AGU), p. 126–140, doi:10.1029/ME004p0126.

Engelhart, S.E., Hemphill-Haley, E., Kelsey, H.M., and Padgett, J.S., 2016, Refined Estimates of Coseismic Subsidence along the Southern Cascadia Subduction Zone in Northern Humboldt Bay (Arcata Bay): Collaborative Research with University of Rhode Island and Humboldt State University: U.S. Geological Survey NERHP Final Technical Report G14AP00128, G14AP00129, 38 p.

Field, M.E., 1993, Liquefaction of Continental Shelf Sediment: The Northern California Earthquake of 1980, *in* Schwab, W.C., Lee, H.J., and Twichell, D.C. eds., Submarine landslides; selected studies in the U.S. Exclusive Economic Zone, Washington, D.C., U.S. Geological Survey Bulletin 2002, Bulletin 2002, p. 143–150.

Field, M.E., 1984, The submarine landslide of 1980 off Northern California, *in* Clarke, S.E. ed., Highlights in Marine Research: U.S. Geological Survey Circular 938, U.S. Geological Survey, p. 65–72.

Field, E.H. et al., 2014, Uniform California Earthquake Rupture Forecast, Version 3 (UCERF3)—The Time-Independent Model: Bulletin of the Seismological Society of America, v. 104, p. 1122–1180, doi:10.1785/0120130164.

Field, M.E., Clarke, S.E., and White, M.E., 1980, Geology and Geologic Hazards of Offshore Eel River Basin, Northern California Continental Margin: U.S. Geological Survey Open-file Report 80-1080, 69 p.

Field, M.E., Gardner, J.V., Jennings, A.E., and Edwards, B.D., 1982, Earthquake-induced sediment failures on a 0.25° slope, Klamath River delta, California: Geology, v. 10, p. 542–546.

Field, M.E., Gardner, J.V., Jennings, A.E., and Edwards, B.D., 1981, Seafloor failures caused by the November 8, 1980 earthquake off northern California: U.S. Geological Survey Open-File Report 81–393.

Field, M.E., and Jennings, A.E., 1987, Seafloor gas seeps triggered by a northern California earthquake: Marine Geology, v. 77, p. 39–51, doi:10.1016/0025-3227(87)90082-X.

Fox, C.G., and Dziak, R.P., 1999, Internal deformation of the Gorda Plate observed by hydroacoustic monitoring: Journal of Geophysical Research: Solid Earth, v. 104, p. 17603–17615.

Freymueller, J.T., Murray, M.H., Segall, P., and Castillo, D., 1999, Kinematics of the Pacific-North America Plate Boundary Zone, northern California: Journal of Geophysical Research: Solid Earth, v. 104, p. 7419–7441, doi:10.1029/1998JB900118.

Fritz, H.M. et al., 2011, Field Survey of the 27 February 2010 Chile Tsunami: Pure and Applied Geophysics, v. 168, p. 1989–2010, doi:10.1007/s00024-011-0283-5.

Fujii, Y., and Satake, K., 2013, Slip Distribution and Seismic Moment of the 2010 and 1960 Chilean Earthquakes Inferred from Tsunami Waveforms and Coastal Geodetic Data: Pure and Applied Geophysics, v. 170, p. 1493–1509, doi:10.1007/s00024-012-0524-2.

Furlong, K.P., and Schwartz, S.Y., 2004, Influence of the Mendocino Triple Junction on the Tectonics of Coastal California: Annual Review of Earth and Planetary Sciences, v. 32, p. 403–433, doi:10.1146/annurev.earth.32.101802.120252.

Garrett, E., Shennan, I., Woodroffe, S.A., Cisternas, M., Hocking, E.P., and Gulliver, P., 2015, Reconstructing paleoseismic deformation, 2: 1000 years of great earthquakes at Chucalén, south central Chile: Quaternary Science Reviews, v. 113, p. 112–122, doi:10.1016/j.quascirev.2014.10.010.

Garrison-Laney, C.E., 1998, Diatom evidence for tsunami inundation from Lagoon Creek, a coastal freshwater pond, Del Norte County, California [Masters Thesis]: Humboldt State University, 108 p., http://dspace.calstate.edu/handle/10211.3/140561 (accessed May 2020).

Goldfinger, C. et al., 2012, Turbidite event history—Methods and implications for Holocene paleoseismicity of the Cascadia subduction zone: U.S. Geological Survey Professional Paper Professional Paper 1661-F, 170 p.

Goldfinger, C., Morey, A.E., Black, B., Beeson, J., Nelson, C.H., and Patton, J., 2013, Spatially limited mud turbidites on the Cascadia margin: segmented earthquake ruptures? Natural Hazards and Earth System Sciences, v. 13, p. 2109–2146, doi:10.5194/nhess-13-2109-2013.

Goldfinger, C., Nelson, C.H., and Johnson, J.E. and, 2003, Holocene earthquake records from the Cascadia subduction zone and northern San Andreas fault based on precise dating of offshore turbidites: Annual Review of Earth and Planetary Sciences, v. 31, p. 555–577, doi:10.1146/annurev.earth.31.100901.141246.

González, F.I., Bernard, E.N., and Satake, K., 1995, The Cape Mendocino Tsunami, 25 April 1992, *in* Tsuchiya, Y. and Shuto, N. eds., Tsunami: Progress in Prediction, Disaster Prevention and Warning, Dordrecht, Springer Netherlands, Advances in Natural and Technological Hazards Research, p. 151–158, doi:10.1007/978-94-015-8565-1_10.

Graehl, N.A., Kelsey, H.M., Witter, R.C., Hemphill-Haley, E., and Engelhart, S.E., 2015, Stratigraphic and microfossil evidence for a 4500-year history of Cascadia subduction zone earthquakes and tsunamis at Yaquina River estuary, Oregon, USA: Geological Society of America Bulletin, v. 127, p. 211–226.

Green, R.K., and Sawyer, T.L., 1993, Geotechnical Aspects of the Petrolia Earthquake, *in* p. 5.

Griffin, W., 1984, Crescent City's dark disaster: Tsunami, March 28, 1964: Crescent City Historical Society, 72 p.

Gulick, S.P.S., Meltzer, A.S., Henstock, T.J., and Levander, A., 2001, Internal deformation of the southern Gorda plate: Fragmentation of a weak plate near the Mendocino triple junction: , p. 4.

Hamilton, S., and Shennan, I., 2005, Late Holocene great earthquakes and relative sea-level change at Kenai, southern Alaska: Journal of Quaternary Science, v. 20, p. 95–111, doi:10.1002/jqs.903.

Harrichhausen, N., Morell, K.D., and Regalla, C., 2024, Forearc faults in northern Cascadia do not accommodate elastic strain driven by the megathrust seismic cycle: Seismica, v. 2, doi:10.26443/seismica.v2i4.1177.

Hartshorn, E.J., Hemphill-Haley, M., Michalak, M., and Crawford, B., 2017, Marine terrace formation associated with northern migration of the Mendocino triple junction at Cape Mendocino, California, *in* p. 304676, doi:10.1130/abs/2017AM-304676.

Hawkes, A.D., Horton, B.P., Nelson, A.R., Vane, C.H., and Sawai, Y., 2011, Coastal subsidence in Oregon, USA, during the giant Cascadia earthquake of AD 1700: Quaternary Science Reviews, v. 30, p. 364–376, doi:10.1016/j.quascirev.2010.11.017.

Heaton, T.H., and Hartzell, S.H., 1987, Earthquake Hazards on the Cascadia Subduction Zone: Science, v. 236, p. 162–168.

Heaton, T.H., and Hartzell, S.H., 1986, Source characteristics of hypothetical subduction earthquakes in the northwestern United States: Bulletin of the Seismological Society of America, v. 76, p. 675–708.

Heaton, T.H., and Kanamori, H., 1984, Seismic potential associated with subduction in the northwestern United States: Bulletin of the Seismological Society of America, v. 74, p. 933–941.

Hemphill-Haley, E., 2017, Observations on the distributions of modern benthic diatoms to improve estimates of past coseismic land-level changes, Humboldt Bay, California: Seismological Research Letters, v. 8, https://www.seismosoc.org/wp-content/uploads/2018/09/srl-2017035.1.pdf.

Hemphill-Haley, E., Kelsey, H.M., Graehl, N., Casso, M., Caldwell, Loofbourrow, C., Robinson, M., Vermeer, J., and Southwick, E., 2019, Recent sandy deposits at five northern California coastal wetlands—Stratigraphy, diatoms, and implications for storm and tsunami hazards: U.S. Geological Survey Scientific Investigations Report USGS Numbered Series 2018–5111, 187 p., http://pubs.er.usgs.gov/publication/sir20185111 (accessed February 2020).

Hill, J.C., Watt, J.T., Brothers, D.S., and Kluesner, J.W., 2020, Submarine canyons, slope failures and mass transport processes in southern Cascadia: Geological Society, London, Special Publications, p. SP500-2019–169, doi:10.1144/SP500-2019-169.

Holzer, T.L., 1992, The Loma Prieta, California, Earthquake of October 17, 1989: Strong ground motion and ground failure: U.S. Geological Survey USGS Professional Paper 1551, http://pubs.er.usgs.gov/publication/pp1551 (accessed April 2020).

Hyndman, R.D., and Wang, K., 1995, The rupture zone of Cascadia great earthquakes from current deformation and the thermal regime: Journal of Geophysical Research: Solid Earth, v. 100, p. 22133–22154, doi:10.1029/95JB01970.

Imakiire, T., and Koarai, M., 2012, Wide-area land subsidence caused by “the 2011 Off the Pacific Coast of Tohoku Earthquake”: Soils and Foundations, v. 52, p. 842–855, doi:10.1016/j.sandf.2012.11.007.

Imbsen, R.A., 1981, Highway structure damage caused by the Trinidad-offshore, California earthquake of November 8, l980: EERI (Earthquake Engineering Research Institute) FHWA/RD-82/017, 35 p., https://trid.trb.org/view/177197 (accessed May 2020).

Jacoby, G.C., Carver, G.A., and Wagner, W., 1995, Trees and herbs killed by an earthquake ~300 yr ago at Humboldt Bay, California: Geology, v. 23, p. 77–80, doi:10.1130/0091-7613(1995)023<0077:TAHKBA>2.3.CO;2.

Keefer, D.K., 1984, Landslides caused by earthquakes: Geological Society of America Bulletin, v. 95, p. 406–421, doi:10.1130/0016-7606(1984)95<406:LCBE>2.0.CO;2.

Kelsey, H.M., and Carver, G.A., 1988a, Late Neogene and Quaternary tectonics associated with northward growth of the San Andreas Transform Fault, northern California: Journal of Geophysical Research: Solid Earth, v. 93, p. 4797–4819, doi:10.1029/JB093iB05p04797.

Kelsey, H.M., and Carver, G.A., 1988b, Late Neogene and Quaternary tectonics associated with northward growth of the San Andreas Transform Fault, northern California: Journal of Geophysical Research: Solid Earth, v. 93, p. 4797–4819, doi:10.1029/JB093iB05p04797.

Kelsey, H.M., Nelson, A.R., Hemphill-Haley, E., and Witter, R.C., 2005, Tsunami history of an Oregon coastal lake reveals a 4600 yr record of great earthquakes on the Cascadia subduction zone: Geological Society of America Bulletin, v. 117, p. 1009–1032.

Kelsey, H.M., Witter, R.C., and Hemphill-Haley, E., 2002, Plate-boundary earthquakes and tsunamis of the past 5500 yr, Sixes River estuary, southern Oregon: Geological Society of America Bulletin, p. 17.

Kelson, K.I., Streig, A.R., Koehler, R.D., and Kang, K.-H., 2006, Timing of Late Holocene paleoearthquakes on the northern San Andreas fault at the Fort Ross Orchard site, Sonoma County, California: Bulletin of the Seismological Society of America, v. 96, p. 1012–1028, doi:10.1785/0120050123.

Kilbourne, R.T., and Saucedo, G.J., 1981, Gorda basin earthquake, northwestern California: California Geology, v. 34, p. 53–57.

Lajoie, K., and Keefer, D., 1981, Investigations of the 8 November 1980 earthquake in Humboldt County, California: U.S. Geological Survey Open-File Report 81–397, 32 p., http://pubs.er.usgs.gov/publication/ofr81397 (accessed March 2020).

Lander, J.F., Lockridge, P.A., and Kozuch, M.J., 1993, Tsunamis affecting the West Coast of the United States, 1806-1992: Washington, D.C., National Oceanic and Atmospheric Administration Publication, National Geophysical Data Center Key to Geophysical Research Documentation No. 29, 242 p.

Lawson, A.C., and Reid, H.F., 1908, The California Earthquake of April 18, 1906: Report of the State Earthquake Investigation Commission: Carnegie Institution of Washington, v. 1, 2, 498 p., http://publicationsonline.carnegiescience.edu/publications_online/earthquake_volume.pdf.

Leonard, L.J., Currie, C.A., Mazzotti, S., and Hyndman, R.D., 2010, Rupture area and displacement of past Cascadia great earthquakes from coastal coseismic subsidence: GSA Bulletin, v. 122, p. 2079–2096, doi:10.1130/B30108.1.

Li, W.-H., 1992, Evidence for the late Holocene coseismic subsidence in the Lower Eel River valley, Humboldt county, Northern California: An application of foraminiferal zonation to indicate tectonic submergence [Masters Thesis]: Humboldt State University.

Litchfield, N.J. et al., 2017, Multiple fault ground surface ruptures in the 14 November 2016 Kaikoura Earthquake, New Zealand (M. Briggs Rich;Hayes, Gavin;Dashti, Shideh;Trainor-Guitton, Whitney;Zellman, Ed.): Seismological Research Letters, v. 88, p. 624-.

Lomax, A., 2005, A reanalysis of the hypocentral location and related observations for the great 1906 California earthquake: Bulletin of the Seismological Society of America, v. 95, p. 861–877.

Løvholt, F., Pedersen, G., Harbitz, C.B., Glimsdal, S., and Kim, J., 2015, On the characteristics of landslide tsunamis: Philosophical transactions. Series A, Mathematical, physical, and engineering sciences, v. 373, doi:10.1098/rsta.2014.0376.

McAdoo, B.G., and Watts, P., 2004, Tsunami hazard from submarine landslides on the Oregon continental slope: Marine Geology, v. 203, p. 235–245, doi:10.1016/S0025-3227(03)00307-4.

McCrory, P.A., 1996, Evaluation of Fault Hazards, Northern Coastal California: US Geological Survey Open-File Report Open-File Report 96–656, 87 p.

McCrory, P.A., 2000, Upper plate contraction north of the migrating Mendocino triple junction, northern California: Implications for partitioning of strain: Tectonics, v. 19, p. 1144–1160, doi:10.1029/1999TC001177.

McLaughlin, R.J., Ellen, S., Blake Jr, M., Jayko, A.S., Irwin, W., Aalto, K., Carver, G., and Clarke Jr, S., 2000, Geology of the Cape Mendocino, Eureka, Garberville, and southwestern part of the Hayfork 30× 60 minute quadrangles and adjacent offshore area, northern California: U.S. Geological Survey Miscellaneous Field Studies Map MF-2336.

Merritts, D.J., 1996, The Mendocino triple junction: Active faults, episodic coastal emergence, and rapid uplift: Journal of Geophysical Research: Solid Earth, v. 101, p. 6051–6070, doi:10.1029/95JB01816.

Milker, Y., Nelson, A.R., Horton, B.P., Engelhart, S.E., Bradley, L.-A., and Witter, R.C., 2016, Differences in coastal subsidence in southern Oregon (USA) during at least six prehistoric megathrust earthquakes: Quaternary Science Reviews, v. 142, p. 143–163, doi:10.1016/j.quascirev.2016.04.017.

Mori, N., Takahashi, T., Yasuda, T., and Yanagisawa, H., 2011, Survey of 2011 Tohoku earthquake tsunami inundation and run-up: Geophysical Research Letters, v. 38, p. 6, doi:10.1029/2011GL049210@10.1002/(ISSN)1944-8007.MEGAQUAKE1.

Murray, M.H., Marshall, G.A., Lisowski, M., and Stein, R.S., 1996, The 1992 M=7 Cape Mendocino, California, earthquake: Coseismic deformation at the south end of the Cascadia megathrust: Journal of Geophysical Research: Solid Earth, v. 101, p. 17707–17725, doi:10.1029/95JB02623.

NASA, 2011, Tohoku Earthquake Shaking Intensity: NASA Earth Observator, https://earthobservatory.nasa.gov/images/49719/tohoku-earthquake-shaking-intensity (accessed May 2020).

NCEI, 2020, Southern Chile Earthquake and Tsunami, 22 May 1960: NOAA National Centers for Environmental Information, https://www.ngdc.noaa.gov/hazard/22may1960.html (accessed May 2020).

NCSS, 2020, Northern California Seismic System: U.C. Berkeley, U.S. Geological Survey: Northern California Seismic System, http://ncedc.org/ncss/ (accessed May 2020).

Nelson, A.R. et al., 1995, Radiocarbon evidence for extensive plate-boundary rupture about 300 years ago at the Cascadia subduction zone: Nature, v. 378, p. 371–374, doi:10.1038/378371a0.

Nelson, A.R., Kashima, K., and Bradley, L.-A., 2009, Fragmentary Evidence of Great-Earthquake Subsidence during Holocene Emergence, Valdivia Estuary, South Central Chile: Bulletin of the Seismological Society of America, v. 99, p. 71–86, doi:10.1785/0120080103.

Nelson, A.R., Kelsey, H.M., and Witter, R.C., 2006, Great earthquakes of variable magnitude at the Cascadia subduction zone: Quaternary Research, v. 65, p. 354–365, doi:10.1016/j.yqres.2006.02.009.

Nicolsky, D.J., Suleimani, E.N., and Hansen, R.A., 2013, Note on the 1964 Alaska Tsunami Generation by Horizontal Displacements of Ocean Bottom. Numerical Modeling of the Runup in Chenega Cove, Alaska: Pure and Applied Geophysics, v. 170, p. 1433–1447, doi:10.1007/s00024-012-0483-7.

Nicovich, S.R., 2015, Latest Pleistocene to Holocene river terrace deformation within the southernmost extent of the Little Salmon fault zone; geomorphic insights to fault termination and rupture history, Van Duzen river, northern California [MS]: Humboldt State University, 85 p.

Niemi, T.M., 2010, Variable earthquake recurrence on the Northern San Andreas fault over the past 3,000 years at the Vedanta marsh site, Olema, CA (Abs.): AGU Fall Meeting Abstracts, v. 41, p. T41C-01.

O'Brien, M.K., 1992, A survey of damage to historic buildings and evaluation of disaster response procedures following the Cape Mendocino earthquakes of April 1992: Cornell Institute for Social and Economic Research Disasters and cultural property, 198 p., https://www.bcin.ca/bcin/detail.app;jsessionid=794EA4C3D1379CC2F434C089DBC155BB?lang=en&id=143241&asq=&csq=&csa=&ps=50&pId=1 (accessed May 2020).

Ogle, B.A., 1953, Geology of the Eel River Basin, Humboldt County, California: California Division of Mines Bulletin 164, 128 p., http://archives.datapages.com/data/bulletns/1953-56/data/pg/0037/0012/2750/2777.htm (accessed February 2020).

Oppenheimer, D. et al., 1993, The Cape Mendocino, California, Earthquakes of April 1992: Subduction at the Triple Junction: Science, v. 261, p. 433–438, doi:10.1126/science.261.5120.433.

Pacific Gas and Electric Company, 2017, Humboldt Bay Independent Spent Fuel Storage Installation - Final Safety Analysis Report Update: NRC Docket No. 72-27, 765 p.

Pacific Gas and Electric Company, 2002, Seismic Assessment for the Humboldt Bay ISFSI Project: Humboldt Bay ISFSI Project Technical Report TR-HBIP-2002-01.

Padgett, J., 2019, CASCADIA SUBDUCTION ZONE COSEISMIC SUBSIDENCE ESTIMATES FROM NORTHERN CALIFORNIA AND WASHINGTON: University of Rhode Island, doi:10.23860/diss-padgett-jason-2019.

Padgett, J.S., Engelhart, S.E., Kelsey, H.M., Witter, R.C., and Cahill, N., 2022, Reproducibility and variability of earthquake subsidence estimates from saltmarshes of a Cascadia estuary: Journal of Quaternary Science, v. 37, p. 1294–1312, doi:10.1002/jqs.3446.

Padgett, J.S., Engelhart, S.E., Kelsey, H.M., Witter, R.C., Cahill, N., and Hemphill-Haley, E., 2021, Timing and amount of southern Cascadia earthquake subsidence over the past 1700 years at northern Humboldt Bay, California, USA: GSA Bulletin, v. 133, p. 2137–2156, doi:10.1130/B35701.1.

Padgett, J.S., Kelsey, H.M., and Lamphear, D., 2019, Upper-plate deformation of Late Pleistocene marine terraces in the Trinidad, California, coastal area, southern Cascadia subduction zone: Geosphere, v. 15, p. 1323–1341, doi:10.1130/GES02032.1.

Patton, J.R., 2004, Late Holocene coseismic subsidence and coincident tsunamis, Southern Cascadia Subduction Zone, Hookton Slough, Wigi (Humboldt Bay), California [Masters Thesis]: Humboldt State University, 85 p., http://dspace.calstate.edu/handle/2148/518 (accessed May 2020).

Personius, S.F., and Nelson, A.R., 2006, Fault number 781, Cascadia megathrust: Quaternary fault and fold database of the United States: U.S. Geological Survey website, https://earthquake.usgs.gov/cfusion/qfault/show_report_AB_archive.cfm?fault_id=781&section_id= (accessed January 2020).

Petersen, M.D. et al., 2020, The 2018 update of the US National Seismic Hazard Model: Overview of model and implications: Earthquake Spectra, v. 36, p. 5–41, doi:10.1177/8755293019878199.

Peterson, C.D., Carver, G.A., Clague, J.J., and Cruikshank, K.M., 2015, Maximum-recorded overland run-ups of major nearfield paleotsunamis during the past 3000 years along the Cascadia margin, USA, and Canada: Natural Hazards, v. 77, p. 2005–2026, doi:10.1007/s11069-015-1689-7.

Peterson, C.D., Carver, G.A., Cruikshank, K.M., Abramson, H.F., Garrison-Laney, C.E., and Dengler, L.A., 2011, Evaluation of the use of paleotsunami deposits to reconstruct inundation distance and runup heights associated with prehistoric inundation events, Crescent City, southern Cascadia margin: Earth Surface Processes and Landforms, v. 36, p. 967–980, doi:10.1002/esp.2126.

Plafker, G., and Savage, J.C., 1970, Mechanism of the Chilean Earthquakes of May 21 and 22, 1960: GSA Bulletin, v. 81, p. 1001–1030, doi:10.1130/0016-7606(1970)81[1001:MOTCEO]2.0.CO;2.

PNSN, 2020, Cascadia Subduction Zone: Pacific Northwest Seismic Network, https://pnsn.org//outreach/earthquakesources/csz (accessed May 2020).

Prentice, C.S., Merritts, D.J., Beutner, E.C., Bodin, P., and Schill, A., 1999, Northern San Andreas fault near Shelter Cove, California: Geological Society of America Bulletin, v. 111, p. 512–523.

Pritchard, C.J., 2004, Late Holocene relative sea-level changes, Arcata Bay, California : evaluation of freshwater syncline movement using coseismically buried soil horizons [Masters Thesis]: Humboldt State University, 63 p., http://dspace.calstate.edu/handle/2148/883 (accessed May 2020).

Reagor, B.G., and Brewer, L.R., 1992, Cape Mendocino Earthquakes of April 25 and 26, 1992: U.S. Geological Survey Open-File Report 92–575, 31 p.

Rollins, J.C., and Stein, R.S., 2010, Coulomb stress interactions among M ≥ 5.9 earthquakes in the Gorda deformation zone and on the Mendocino Fault Zone, Cascadia subduction zone, and northern San Andreas Fault: Journal of Geophysical Research, v. 115, p. 1–19, doi:10.1029/2009JB007117.

Rukstales, K.S., and Shumway, A.M., 2019, Data Release for 2018 Update of the U.S. National Seismic Hazard Model:, doi:10.5066/P9WT5OVB.

Satake, K., and Atwater, B.F., 2007, Long-term perspectives on giant earthquakes and tsunamis at subduction zones: Annual Review of Earth and Planetary Sciences, v. 35, p. 26, doi:10.1146/annurev.earth.35.031306.140302.

Satake, K., Shimazaki, K., Tsuji, Y., and Ueda, K., 1996, Time and size of a giant earthquake in Cascadia inferred from Japanese tsunami records of January 1700: Nature, v. 379, p. 246–249, doi:10.1038/379246a0.

Satake, K., Wang, K., and Atwater, B.F., 2003, Fault slip and seismic moment of the 1700 Cascadia earthquake inferred from Japanese tsunami descriptions: Journal of Geophysical Research: Solid Earth, v. 108, doi:10.1029/2003JB002521.

Savage, J.C., Lisowski, M., and Prescott, W.H., 1991, Strain accumulation in western Washington: Journal of Geophysical Research: Solid Earth, v. 96, p. 14493–14507, doi:10.1029/91JB01274.

Savage, J.C., and Plafker, G., 1991, Tide gage measurements of uplift along the south coast of Alaska: Journal of Geophysical Research: Solid Earth, v. 96, p. 4325–4335, doi:10.1029/90JB02540.

Schulz, S.S., and Wallace, R.E., 1997, The San Andreas Fault: U.S. Geological Survey General Interest Publication 3, https://pubs.usgs.gov/gip/earthq3/.

Schwartz, S.Y., and Hubert, A., 1997, The state of stress near the Mendocino Triple Junction from inversion of earthquake focal mechanisms: Geophysical Research Letters, v. 24, p. 1263–1266, doi:10.1029/97GL01060.

Schwartz, D.P., Lienkaemper, J.J., Hecker, S., Kelson, K.I., Fumal, T.E., Baldwin, J.N., Seitz, G.G., and Niemi, T.M., 2014, The Earthquake Cycle in the San Francisco Bay Region: A.D. 1600–2012: Bulletin of the Seismological Society of America, v. 104, p. 1299–1328, doi:10.1785/0120120322.

Shelly, D.R., Goldberg, D.E., Materna, K.Z., Skoumal, R.J., Hardebeck, J.L., Yoon, C.E., Yeck, W.L., and Earle, P.S., 2024, Subduction intraslab-interface fault interactions in the 2022 M_w 6.4 Ferndale,

California, earthquake sequence: Science Advances, v. 10, p. eadl1226, doi:10.1126/sciadv.adl1226.

Shennan, I., and Hamilton, S., 2006, Coseismic and pre-seismic subsidence associated with great earthquakes in Alaska: Quaternary Science Reviews, v. 25, p. 1–8, doi:10.1016/j.quascirev.2005.09.002.

Smith, S.W., Knapp, J.S., and McPherson, R.C., 1993, Seismicity of the Gorda Plate, structure of the continental margin, and an eastward jump of the Mendocino Triple Junction: Journal of Geophysical Research: Solid Earth, v. 98, p. 8153–8171, doi:10.1029/93JB00026.

Song, S.G., Beroza, G.C., and Segall, P., 2008, A Unified Source Model for the 1906 San Francisco Earthquake: Bulletin of the Seismological Society of America, v. 98, p. 823–831, doi:10.1785/0120060402.

Stein, R.S., Rollins, C., and Sevilgen, V., 2023, December 2022 California earthquake ruptured unknown fault: an analysis: Temblor, https://temblor.net/earthquake-insights/dec-2022-california-earthquake-unknown-fault-analysis-14867/.

Stoddard, P.R., 1991, A comparison of brittle deformation models for the Gorda plate: Tectonophysics, v. 187, p. 205–214, doi:10.1016/0040-1951(91)90420-W.

Stoffer, P.W., 2005, The San Andreas Fault In The San Francisco Bay Area, California: A Geology Fieldtrip Guidebook To Selected Stops On Public Lands: U.S. Geological Survey Open-file Report 2005–1127, 133 p., https://pubs.usgs.gov/of/2005/1127/ (accessed April 2020).

Storesund, R., Dengler, L.A., Mahin, S., Collins, B.D., Hanshaw, M., Turner, F., and Welsh, K., 2010, M6.5 earthquake offshore Northern California, January 9, 2010: Field Reconnaissance Summary: Geotechnical Extreme Events Reconnaissance (GEER) Association GEER Reconnaissance Report, February 12, 2010, 41 p.

Stover, C.W., and Coffman, J.L., 1993, Seismicity of the United States, 1568-1989 (Revised): Washington, D.C., U.S. Geological Survey Professional Paper 1527, Professional Paper 1527, 418 p.

Streig, A.R., Dawson, T.E., and Weldon, R.J., 2014, Paleoseismic Evidence of the 1890 and 1838 Earthquakes on the Santa Cruz Mountains Section of the San Andreas Fault, near Corralitos, California: Bulletin of the Seismological Society of America, v. 104, p. 285–300, doi:10.1785/0120130009.

Sugawara, D., Minoura, K., and Imamura, F., 2008, Chapter Three - Tsunamis and Tsunami Sedimentology, *in* Shiki, T., Tsuji, Y., Yamazaki, T., and Minoura, K. eds., Tsunamiites, Amsterdam, Elsevier, p. 9–49, doi:10.1016/B978-0-444-51552-0.00003-5.

Suppasri, A., Fukutani, Y., Abe, Y., and Imamura, F., 2011, Relationship between earthquake magnitude and tsunami height along the Tohoku coast based on historical tsunami trace database and the 2011 Great East Japan Tsunami: Report of Tsunami Engineering, v. 30, p. 37–49.

Swan, F.H., Carver, G.A., McLaren, M., and Page, W.D., 2002, Seismic Hazard Assessment for the Humboldt Bay ISFSI Project: Regional Geology and Seismology: Pacific Gas and Electric Company Technical Report TR-HBIP-2002-01, Section 3, 83 p.

Thatcher, W., Marshall, G., and Lisowski, M., 1997, Resolution of fault slip along the 470-km-long rupture of the great 1906 San Francisco earthquake and its implications: Journal of Geophysical Research: Solid Earth, v. 102, p. 5353–5367, doi:10.1029/96JB03486.

Tobin, D.G., and Sykes, L.R., 1968, Seismicity and tectonics of the northeast Pacific Ocean: Journal of Geophysical Research (1896-1977), v. 73, p. 3821–3845, doi:10.1029/JB073i012p03821.

Toppozada, T.R., and Borchardt, G., 1998, Re-evaluation of the 1836 “Hayward fault” and the 1838 San Andreas fault earthquakes: Bulletin of the Seismological Society of America, v. 88, p. 140–159.

Toppozada, T., and Branum, D., 2004, California earthquake history: Annals of Geophysics, v. 47, doi:10.4401/ag-3317.

Tsuji, Y., Satake, K., Ishibe, T., Harada, T., Nishiyama, A., and Kusumoto, S., 2014, Tsunami Heights along the Pacific Coast of Northern Honshu Recorded from the 2011 Tohoku and Previous Great Earthquakes: Pure and Applied Geophysics, v. 171, p. 3183–3215, doi:10.1007/s00024-014-0779-x.

US Geological Survey, 2021, M 6.2 - 7km N of Petrolia, CA:, https://www.usgs.gov/media/images/map-showing-revised-location-m62-petrolia-earthquake-12202021.

US Geological Survey, 2022, M6.4 - 15 km WSW of Ferndale, CA:, https://earthquake.usgs.gov/earthquakes/eventpage/nc73821036/executive.

USGS, 2020a, Earthquake Magnitude, Energy Release, and Shaking Intensity: U.S. Geological Survey Earthquake Hazards, https://www.usgs.gov/natural-hazards/earthquake-hazards/science/earthquake-magnitude-energy-release-and-shaking-intensity?qt-science_center_objects=0#qt-science_center_objects (accessed April 2020).

USGS, 2020b, M 6.5 - Northern California (1954-12-21 19:56:24 (UTC)): U.S. Geological Survey Earthquake Hazards Program, https://earthquake.usgs.gov/earthquakes/eventpage/ushis2000/executive (accessed June 2020).

USGS, 2020c, M 6.5 - offshore Northern California (1992-04-26 07:41:40 (UTC)): U.S. Geological Survey Earthquake Hazards Program, https://earthquake.usgs.gov/earthquakes/eventpage/nc268031/executive (accessed May 2020).

USGS, 2020d, M 6.5 - offshore Northern California (2010-01-10 00:27:39 (UTC)): U.S. Geological Survey Earthquake Hazards Program, https://earthquake.usgs.gov/earthquakes/eventpage/nc71338066/executive (accessed May 2020).

USGS, 2020e, M 6.6 - offshore Northern California (1992-04-26 11:18:25 (UTC)): U.S. Geological Survey Earthquake Hazards Program, https://earthquake.usgs.gov/earthquakes/eventpage/nc268078/executive (accessed May 2020).

USGS, 2020f, M 7.2 - offshore Northern California (1980-11-08 10:27:34 (UTC)): USGS Earthquake Hazards Program, https://earthquake.usgs.gov/earthquakes/eventpage/usp0001aq1/executive (accessed May 2020).

USGS, 2020g, M 7.9 - The 1906 San Francisco Earthquake:, https://earthquake.usgs.gov/earthquakes/eventpage/iscgem16957905/map (accessed April 2020).

USGS, 2020h, M 9.3 Scenario Earthquake - Cascadia Megathrust - whole CSZ Characteristic largest M branch: USGS Earthquake Hazards Program, https://earthquake.usgs.gov/scenarios/eventpage/bssc2014cascadia_sub0_m9p34_se/region-info (accessed May 2020).

USGS, 2020i, Search Earthquake Catalog: U.S. Geological Survey Earthquake Hazards Program, https://earthquake.usgs.gov/earthquakes/search/ (accessed May 2020).

USGS, 2020j, The Great 1906 San Francisco Earthquake: U.S. Geological Survey Earthquake Hazards Program, https://earthquake.usgs.gov/earthquakes/events/1906calif/18april/index.php (accessed April 2020).

USGS, 2020k, The Modified Mercalli Intensity Scale: U.S. Geological Survey Earthquake Hazards, https://www.usgs.gov/natural-hazards/earthquake-hazards/science/modified-mercalli-intensity-scale?qt-science_center_objects=0#qt-science_center_objects (accessed February 2020).

Valentine, D.W., 1992, Late Holocene Stratigraphy, Humboldt Bay, California: Evidence for Late Holocene Paleoseismicity of the Southern Cascadia Subduction Zone [Masters Thesis]: Humboldt State University, https://escholarship.org/uc/item/7328g533 (accessed May 2020).

Valentine, D.W., Keller, E.A., Carver, G., Li, W.-H., Manhart, C., and Simms, A.R., 2012, Paleoseismicity of the Southern End of the Cascadia Subduction Zone, Northwestern California: Bulletin of the Seismological Society of America, v. 102, p. 1059–1078, doi:10.1785/0120110103.

Velasco, A.A., Ammon, C.J., and Lay, T., 1994, Recent large earthquakes near Cape Mendocino and in the Gorda plate: Broadband source time functions, fault orientations, and rupture complexities: Journal of Geophysical Research: Solid Earth, v. 99, p. 711–728, doi:10.1029/93JB02390.

Vermeer, J., 2016, Interseismic lithospheric response of the southern end of the Cascadia subduction zone since the 1992 Cape Mendocino M 7.1 earthquake [Masters Thesis]: Humboldt State University, 82 p., http://humboldt-dspace.calstate.edu/bitstream/handle/10211.3/175467/Vermeer_Jessica_Sp2016.pdf?sequence=1.

Vermeer, J., Crawford, B., and Hemphill-Haley, M.A., 2015, Vertical crustal stability in 23 years since the 1992 Cape Mendocino M 7.1 earthquake: benchmark survey results, interpretations and tectonic implications: AGU Fall Meeting Abstracts, v. 31, p. T31B-2890.

Vermeer, J., and Hemphill-Haley, M.A., 2014, Interseismic lithospheric response of the southern end of the Cascadia subduction zone following the 1992 Cape Mendocino earthquake: AGU Fall Meeting Abstracts, v. 11, p. G11A-0474.

Vick, G., 1988, Late Holocene Paleoseismicity and relative vertical crustal movements [Masters Thesis]: Humboldt State University, 96 p.

Voit, S.S., 1987, Tsunamis: Annual Review of Fluid Mechanics, v. 19, p. 217–236, doi:10.1146/annurev.fl.19.010187.001245.

Wallace, R.E. (Ed.), 1990, The San Andreas Fault System, California: U.S. Geological Survey Professional Paper 1515, 312 p., https://pubs.usgs.gov/pp/1990/1515/.

Wang, K., and Tréhu, A.M., 2016, Invited review paper: Some outstanding issues in the study of great megathrust earthquakes—The Cascadia example: Journal of Geodynamics, v. 98, p. 1–18, doi:10.1016/j.jog.2016.03.010.

Wang, K., Wells, R.E., Mazzotti, S., Hyndman, R.D., and Sagiya, T., 2003, A revised dislocation model of interseismic deformation of the Cascadia subduction zone: Journal of Geophysical Research B: Solid Earth, v. 108, doi:10.1029/2001JB001227.

Watt, J., Ponce, D., Parsons, T., and Hart, P., 2016, Missing link between the Hayward and Rodgers Creek faults: Science Advances, v. 2, p. e1601441, doi:10.1126/sciadv.1601441.

Watts, P.M., 2002, Probabilities and characteristics of tsunamigenic underwater landslides and slumps, doi:10.3133/b2002.

Weldon, R.J., Dawson, T.E., Biasi, G., Madden, C., and Streig, A.R., 2013, Appendix G—Paleoseismic Sites Recurrence Database, *in* Uniform California Earthquake Rupture Forecast, Version 3 (UCERF3)—The Time-Independent Model, U.S. Geological Survey Open-file Report 2013-1165, Open-file Report 2013-1165, p. 73.

Wells, D.L., and Coppersmith, K.J., 1994, New empirical relationships among magnitude, rupture length, rupture width, rupture area, and surface displacement: Bulletin of the Seismological Society of America, v. 84, p. 974–1002.

Wilson, D.S., 1989, Deformation of the so-called Gorda Plate: Journal of Geophysical Research: Solid Earth, v. 94, p. 3065–3075, doi:10.1029/JB094iB03p03065.

Wilson, D.S., 2012, Deformation of the so-called Gorda Plate: Journal of Geophysical Research: Solid Earth, p. 3065–3075, doi:10.1029/JB094iB03p03065@10.1002/(ISSN)2169-9356.MENDOCINO1.

Witter, R.C., Kelsey, H.M., and Hemphill-Haley, E., 2003, Great Cascadia earthquakes and tsunamis of the past 6700 years, Coquille River estuary, southern coastal Oregon: Geological Society of America Bulletin, v. 115, p. 1289–1306.

Witter, R.C., Kelsey, H.M., and Hemphill-Haley, E., 2001, Pacific storms, El Nino and tsunamis: competing mechanisms for sand deposition in a coastal marsh, Euchre Creek, Oregon: Journal of Coastal Research, p. 563–583.

Witter, R.C., Patton, J.R., Carver, G.A., Kelsey, H.M., Garrison-Laney, C., Koehler, R.D., and Hemphill-Haley, E., 2002, Upper Plate Earthquakes on the Western Little Salmon Fault and Contemporaneous Subsidence of Southern Humboldt Bay Over the Past 3,600 Years: US Geological Survey National Earthquake Hazards Reduction Program NEHRP Final Technical Report 01HQGR0125.

Wong, I.G., 2005, Low Potential for Large Intraslab Earthquakes in the Central Cascadia Subduction Zone: Bulletin of the Seismological Society of America, v. 95, p. 1880–1902, doi:10.1785/0120040132.

Woodward-Clyde Consultants, 1980, Evaluation of the potential for resolving the geologic and seismic issues at the HBPP Unit No. 3: Summary to Pacific Gas and Electric company, San Francisco, CA:, 74, plus appendix p.

Yeck, W.L., Shelly, D.R., Materna, K.Z., Goldberg, D.E., and Earle, P.S., 2023, Dense geophysical observations reveal a triggered, concurrent multi-fault rupture at the Mendocino Triple Junction: Communications Earth & Environment, v. 4, p. 94, doi:10.1038/s43247-023-00752-2.

Yoon, C.E., and Shelly, D.R., 2024, Distinct Yet Adjacent Earthquake Sequences near the Mendocino Triple Junction: 20 December 2021 Mw 6.1 and 6.0 Petrolia, and 20 December 2022 Mw 6.4 Ferndale: The Seismic Record, v. 4, p. 81–92, doi:10.1785/0320230053.

Youd, T.L., and Hoose, S.N., 1978, Historic ground failures in northern California triggered by earthquakes: U.S. Geological Survey USGS Professional Paper 998, 194 p.

Zhang, H., Niemi, T., and Fumal, T., 2006, A 3000-year record of earthquakes on the northern San Andreas fault at the Vedanta marsh site, Olema, California: Seismological Research Letters, v. 77, p. 176.

Zimmerman, R. et al., 2005, Cascadia subduction zone earthquakes: a magnitude 9.0 earthquake scenario: Oregon Department of Geology and Mineral Industries, Cascadia Region Earthquake Workgroup, 24 p.